

**Design and Construction of a Sample Holder and Heater Apparatus for
Thin Film Stress Measurements.**

By

Adam R. Silvernail

A thesis submitted in partial fulfillment of the requirements for
the degree of

Bachelor of Science

Houghton College

September 2011

Signature of Author

Department of Physics
September 1, 2011

.....
Dr. Brandon Hoffman
Assistant Professor of Physics
Research Supervisor

.....
Dr. Christopher Wells
Assistant Professor of Physics

Design and Construction of a Sample Holder and Heater Apparatus for Thin Film Stress Measurements.

By

Adam R. Silvernail

Submitted to the Houghton College Department of Physics
on September 23, 2011 in partial fulfillment of the requirement for
the degree of Bachelor of Science

Abstract

Thin film stress may be characterized through curvature measurements due to film strain. One way to change and control film stress is through a change in temperature while the film and substrate have varying coefficients of thermal expansion. To control the temperature of the film/substrate system, a sample holder and heater have been constructed for the Houghton College deposition chamber. Samples will be heated while under vacuum while measuring the resulting change in film/substrate curvature as a function of temperature for various materials, such as silver and titanium, using an interferometer. Film stress may be calculated directly from the film curvature using appropriate models such as the Stoney formula. Various models for relating curvature and stress will be discussed, as well as a description of the Houghton College deposition apparatus.

Thesis Supervisor: Dr. Brandon Hoffman

Title: Assistant Professor of Physics

TABLE OF CONTENTS

TABLE OF FIGURES5

Chapter 1 : HISTORY AND MOTIVATION6

1.1 Introduction6

1.2 Thin Film Stress7

1.2.1 Definition of Stress in Thin Films7

1.2.2 Causes of Stress in Thin Films7

1.2.3 Effect of Stress in Thin Films7

1.2.4 History of Characterizing Stress.....8

1.3 Houghton College Research8

Chapter 2 : THEORY OF STRESS IN THIN FILMS9

2.1 Thin film Stresses.....9

2.1.1 Introduction9

2.1.2 Physics of Stresses9

2.1.3 Thermal Stresses.....13

2.2 Measuring Stresses13

2.2.1 Relating Curvature to Stress.....13

2.2.2 Stoney formula14

2.2.3 Extensions to Stoney Formula17

2.2.3.1 Film thickness on order of substrate thickness17

2.2.3.2 Non-linear Model with Bifurcation17

2.2.3.3 Relaxing assumptions of Stoney Formula18

2.2.4 Methods for Measuring Curvature19

Chapter 3 : DEPOSITION APPARATUS.....22

3.1 Introduction22

3.2 Deposition Apparatus22

3.2.1 Purpose22

3.2.2 Description.....23

3.2.3 Deposition Vacuum Chamber.....24

3.2.4 Vacuum System25

3.2.5 Sample Holder and Heater Apparatus26

3.2.6	Ion Gun	27
3.2.7	Evaporation System and Deposition Rate Monitor	27
3.2.8	Shutters	29
3.2.9	Interferometer	30
3.3	Sample Holder and Heater.....	32
3.3.1	Sample Holder.....	32
3.3.1.1	Sample Holder Design Choices.....	33
3.3.2	Sample Heater.....	35
3.3.3	Thermal Insulative Shielding	39
Chapter 4 : FUTURE EXPERIMENTS AND CONSIDERATIONS.....		40
4.1	Current Status - 2011.....	40
4.2	Future Goals.....	40
Appendix A : EXPERIMENTAL PROCEDURE		42
A.1	Goals for Deposition Experiments.....	42
A.2	Preparing for Deposition	42
A.2.1	Placing Substrate into Sample Chamber.....	42
A.2.2	Bringing System to Vacuum	43
A.2.3	Ion Cleaning.....	43
A.3	Deposition Procedure	44
A.3.1	Preparing Evaporation System.....	44
A.3.2	Aligning Shutters for Thickness Gradient.....	44
A.3.3	Performing Deposition	45
A.4	Post Deposition.....	45
A.5	Heating Experiments	45
A.5.1	Applications of Sample Heater.....	45
A.5.2	Sample Heater Procedure.....	46
A.5.3	Interferometer Experiments	46
REFERENCES		47

TABLE OF FIGURES

<i>Figure 1: Depiction of thin film material compared to its corresponding bulk form.</i>	6
<i>Figure 2: Geometrical representation of the components of stress, σ, in rectangular coordinates.</i>	9
<i>Figure 3: Thin film adhered to a substrate with infinitesimal point expanded to show the components of stress.</i>	10
<i>Figure 4 : An example of stress of a thin film and opposing stress of a substrate in the radial direction.</i>	11
<i>Figure 5: A one-dimensional example of strain (ϵ) caused by stress (σ).</i>	11
<i>Figure 6: Demonstrating the behavior of the axial and transverse strain of a material while under tensile stress.</i>	12
<i>Figure 7: Thin film and substrate initially with length L expand differing amounts in one dimension.</i>	14
<i>Figure 8: Two-dimensional example of curvature (κ) due to varying strain of a thin film and substrate.</i>	14
<i>Figure 9: Graphical demonstration of proportionality of $\epsilon z = \delta a = zR$.</i>	15
<i>Figure 10: Harper model of curvature due to stress showing bifurcation beyond critical point of $S = 1.43$.</i>	18
<i>Figure 11: Concept behind laser deflectometry.</i>	20
<i>Figure 12: Coherent Grade Sensing (CGS) layout.</i>	21
<i>Figure 13: 3D model of chamber and interferometer suspended by springs.</i>	22
<i>Figure 14: Houghton College Deposition Apparatus suspension system.</i>	23
<i>Figure 15: Current external view of deposition chamber.</i>	24
<i>Figure 16: Two dimensional internal diagram of deposition chamber with all components labeled.</i>	25
<i>Figure 17 : Images of sample holder and heater apparatus outside of the chamber.</i>	26
<i>Figure 18: Diagram of gridless ion gun, which ionizes and accelerates gas particles towards the substrate.</i>	27
<i>Figure 19: Two-dimensional representation of thermal evaporation system.</i>	28
<i>Figure 20: Deposition rate monitor.</i>	29
<i>Figure 21 : Diagram of laser interferometer and deposition chamber.</i>	30
<i>Figure 22: Interference precision required to be stable for CCD pixel measurements of the interferometer.</i>	31
<i>Figure 23: Diagram of sample holder and heater while attached to the roof of the chamber.</i>	32
<i>Figure 24: Dimensions of sample holder components, drawn to scale.</i>	33
<i>Figure 25: Top down view of sample holder with dimensions of sample, sample holder, and hole in chamber.</i>	34
<i>Figure 26: Sample heater with tungsten wire threaded in circular pattern throughout the ceramic plate.</i>	35
<i>Figure 27: Side view of one interweaving pattern used for wiring the tungsten filament for the sample heater.</i>	36
<i>Figure 28: Alternate tungsten wire weaving pattern for maximizing ratio of heater wire on film side of heater.</i>	36
<i>Figure 29 : Sample holder and heater with shielding and electronics.</i>	37
<i>Figure 30: Close up of sample heater and molybdenum shielding with dimensions.</i>	38
<i>Figure 31: Proposed interferometer apparatus diagram with laser path highlighted in red.</i>	41

Chapter 1 : HISTORY AND MOTIVATION

1.1 Introduction

Thin metal films are a form of material used in many applications, ranging from microelectronics, optics, and protective or decorative coatings [1]. Specifically, thin films are thin sheets of material that range in thickness on the order nanometers and micrometers, even being as few as several atoms thick. The study of thin films provides better understanding of their structural behavior for their applications, and the understanding of materials on the atomic scale. Over the past several decades, significant progress has been made to improve models for the behavior of thin films, providing understanding of thin film material properties which differ from the respective bulk form [2]. The Houghton College Physics Department is interested in studying these unique properties and is presently developing an apparatus to develop metal thin film materials and analyze them through various mechanisms to be described in this thesis.

Thin films have unique properties differing from their bulk form, making them a key subject of research interest. A depiction of thin film material is shown in Figure 1, as compared to bulk material. Thin films are not structurally stable and typically need to have a rigid substrate to provide support for formation, as can be seen in Figure 3. However, the structural strength of thin films can be quite large relative to their size, allowing them to experience and exert tremendous stress relative to their thickness which can be measured indirectly through macroscopic measurements of the film displacement strain due to the stress [3].

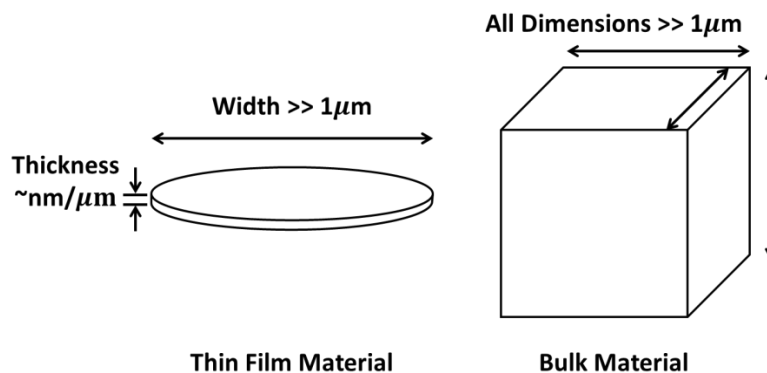


Figure 1: Depiction of thin film material compared to its corresponding bulk form. Thin films are defined by having thickness on the order of nm and μm . In bulk form, all dimensions are considered to be on the macroscopic scale.

1.2 Thin Film Stress

1.2.1 Definition of Stress in Thin Films

All materials, particularly thin films, experience stress to some magnitude. Stress represents the internal forces between atoms in a lattice structure due to intrinsic properties and application of external forces. Stresses in thin films are defined by the internal force per unit area in the direction of the respective principle axes of the film, and is further described in Section 2.1.

1.2.2 Causes of Stress in Thin Films

Stress is known to occur through a variety of mechanisms, including during film deposition and through a changing physical environment. Examples of these mechanisms include, surface or interface mismatch stress during deposition, grain growth and impurities in film, temperature change when the coefficients of expansion of bonded materials are different, exerted electromagnetic or gravitational forces, and chemical reactions [4]. Film stress directly depends on the material composition of the thin film, the thickness of the film, and the uniformity of the film. All thin films exhibit a net internal stress which can be large relative to the thickness of the film, so the stress is a vital factor for the film's properties [5].

1.2.3 Effect of Stress in Thin Films

Stress can cause changes in the structure and strength of thin films and influence its adhesiveness to a bonding material. Specifically, stress can cause the material to shift and displace in reaction to the force associated with it. This displacement may be defined as strain, which may be measured and analyzed to identify the stress which caused it; strain is further discussed in Section 2.1.2. Stress can be the cause of thin film cracking, hillocking, or even delamination from its bonding surface which can result in failing components [6]. However, small levels of stress can sometimes improve adhesiveness in electronic applications, making stress a useful tool for increasing component longevity [7].

Stress can also influence the microstructure of atoms in the film, thus changing the grain orientation while experiencing varying amounts of stress. This effect was studied by Houghton College in collaboration with Shefford Baker at Cornell University and the Cornell Center for Materials Research during the summers of 2007-2009. Thin silver films were manufactured and their grain structure was studied under varying conditions of silver thickness, titanium capping layer thickness, and annealing time and temperature. Results show that the grain structure is indeed affected by each of these varying conditions due to their influence on the film stress [8].

Finally, the strain due to stress can affect the overall structure of the film and bonding surface, otherwise known as a substrate, causing the surface bend and flex to a curved equilibrium position, as described in Section 2.2, which is an important consequence for materials that are intended to remain flat. This film/substrate curvature is a useful indicator of film stress, and may be measured directly to indirectly determine the stress that caused it.

1.2.4 History of Characterizing Stress

A pioneer of thin film research, G.G. Stoney published a paper in 1909 which introduced an analytical linear model for relating thin film stress to the curvature geometry of the film while adhered to a substrate. Stoney developed his model using the simple ideal case of a uniform film with thickness much less than the substrate thickness, where the stress is laterally uniform and edge effects of the film and substrate are inconsequential, and the curvature is also spherical and uniform [9]. This model can serve as a basic analytical tool for characterizing film stress from the resulting film and substrate curvature, but it is not suitable for practical applications with films that are not ideal. Consequently, efforts have been made to revise Stoney's linear model into a non-linear model and allow it to be applied for varying conditions such as non-uniform film thickness, varying film and substrate shape, using different layers of film and substrate, as well as radially symmetric temperature gradients and edge effects[10,11,12,13]. Film stress is being studied more recently for its consequences in thin film applications and new models are being developed to improve understanding of film behavior and predict stress levels more accurately than Stoney's model. When appropriately applied, the Stoney model still provides a reasonably reliable thin film stress analysis and will be a good starting model for thin films research at Houghton College.

1.3 Houghton College Research

Houghton College is undergoing a project for manufacturing thin films and analyzing them for their structural properties, namely their curvature due to internal film stress. Using a deposition apparatus and interferometer, films may be made and tested all in one system. Specifically, films with varying thickness and composition can be tested under varying temperature to observe the change in curvature due to thermal stress. Construction of the components has been recently completed in 2011, with much testing needed before the apparatus may be ready for full operation.

Chapter 2 : THEORY OF STRESS IN THIN FILMS

2.1 Thin film Stresses

2.1.1 Introduction

Thin film systems are always under a state of stress which affects their structural properties and behavior accordingly. This behavior may be observed and analyzed to better understand the origin and physics of stress in thin film materials which differ from bulk materials. This chapter will explore certain film properties through various characterizations and introduce models which continue to further understanding of thin film materials with each revision.

2.1.2 Physics of Stresses

Stress is defined by the amount of force exerted within a perpendicular area such that,

$$\bar{\sigma} = \frac{F}{A} \quad \text{or} \quad \sigma = \frac{dF}{dA} \quad [1]$$

where $\bar{\sigma}$ is the mean stress over a finite area and σ is the point-wise stress value. Stress has the units of pressure, but is conventionally defined as a three dimensional tensor ($\sigma_{ij} = \frac{dF_i}{dA_j}$), for a given point in a material. For the sake of discussion, we will consider all shear stress ($i \neq j$) to be negligible, thus the convention will be to drop the second repeated index, ($\sigma_{ii} \equiv \sigma_i$). Stress may be defined in terms of components of principle axes, such as seen in Figure 2.

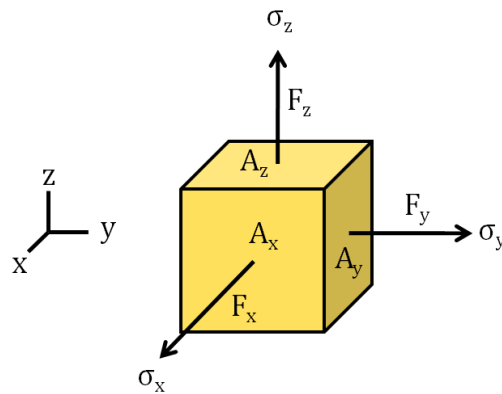


Figure 2: Geometrical representation of the components of stress, σ , in rectangular coordinates, which is determined by the total force, F , applied over an area, A .

For a thin film, it is common to assign the principle axes to be in cylindrical coordinates, as seen in Figure 3. Generally, the stress component perpendicular to the plane of a thin film (σ_z), otherwise called the out-of-plane stress, is assumed to be negligible if the film is in equilibrium, such that there

are negligible external forces acting on it. This assumption is applied to the various models described in section 2.2.

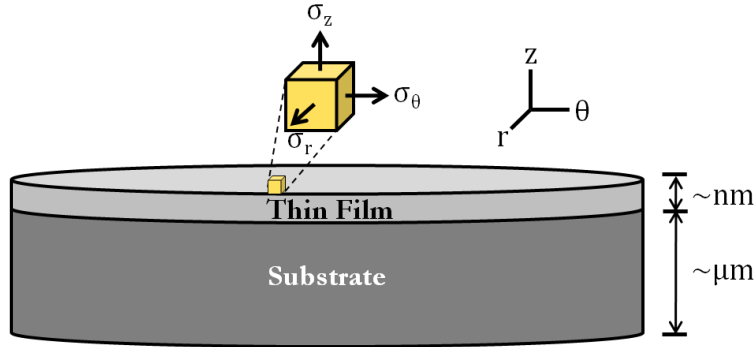


Figure 3: Thin film adhered to a substrate with infinitesimal point expanded to show the components of stress of that point. In cylindrical coordinates, the principle axes determine the stress components, σ_r , σ_θ , and σ_z . The thickness of the substrate is on the order of micrometers and the thickness of the thin film is generally on the order of nanometers.

Stress occurs throughout a material, distributing itself according to the interactions of particles in the material. In the context of thin films, stress arises from the interaction between the thin film and substrate interface. Depending on the lattice structure of the thin film and substrate, there may be a mismatch stress at the interface; an example is shown in Figure 4. Stress is often not uniform in magnitude or direction as is shown in these introductory examples; however, it may be approximated to be so for the various models to be discussed in Section 2.2. The magnitude of stress in a material will determine the amount of displacement which is exhibited by Hooke's Law in one dimension as,

$$\sigma_m = \varepsilon_m M_f, \quad [2]$$

where σ_m is the mean stress component causing the strain or displacement, ε_m , and M_f is the biaxial elastic modulus of the film material to be examined later in this section. This relationship shows that stress and strain affect each other linearly, with a proportionality constant depending on the material, M_f . Stress may be generally referred to as either compressive or tensile depending on the direction of the internal forces. Compressive stress refers to the internal forces of the material acting inwardly whereas tensile stress refers to the internal forces acting outwardly. Figure 4 shows both kinds of stress, where the black arrows illustrate compressive stress and red arrows illustrate tensile stress of either the substrate or thin film. A combination of compressive or tensile stress may be present in a thin film/substrate system, and is indicated by the sign of the stress at any given point. The net stress affects the behavior of the film as it comes to equilibrium, specifically through strain.

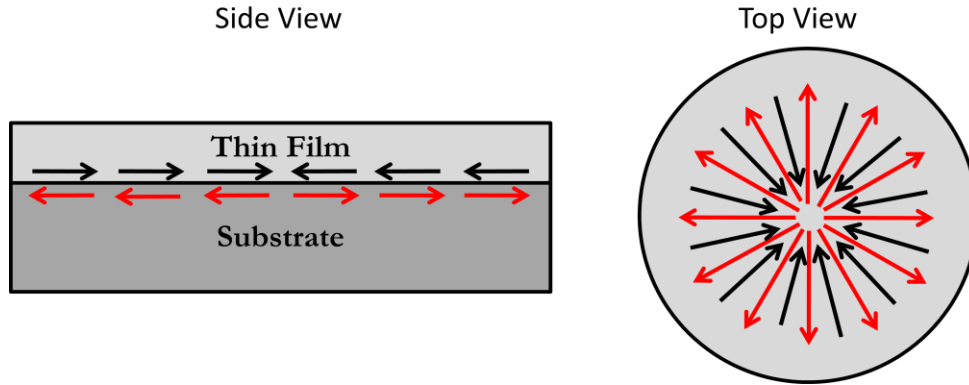


Figure 4 : An example of stress of a thin film and opposing stress of a substrate in the radial direction. The thin film is under compressive stress while the substrate is under an equivalent tensile stress. The film stress direction is labeled by black arrows and the substrate stress direction is labeled by red arrows.

Strain (ϵ) is defined by the ratio of displacement of a material under stress such that,

$$\epsilon = \frac{\Delta L}{L}. \quad [3]$$

Strain occurs by the material stretching or shifting to reach an equilibrium state due to the intrinsic film stress or external forces acting on it. Strain is unitless, allowing its value to be scalable for any material size or dimension. An example of a material experiencing a one-dimensional strain from a tensile stress is shown in Figure 5.

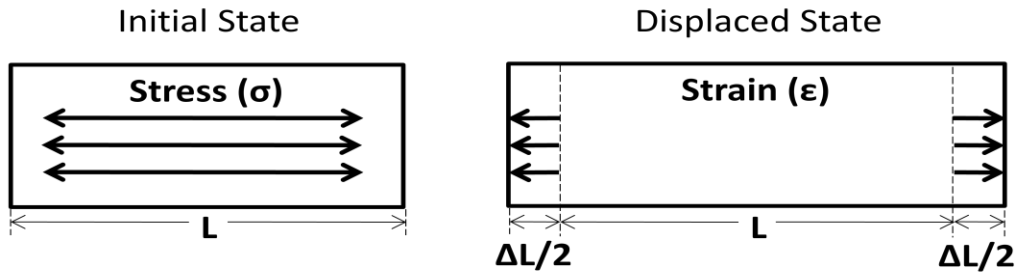


Figure 5: A one-dimensional example of strain (ϵ) caused by stress (σ). When a material under stress is not in an equilibrium state, a resulting strain occurs which is defined by the ratio of displacement (ΔL) with respect to its initial length (L).

Strain in thin films depends on the material's elastic properties. In one dimension, the uniaxial relationship between stress and strain is known as Young's modulus (Y) where,

$$Y = \frac{\sigma_{\text{axial}}}{\epsilon_{\text{axial}}}. \quad [4]$$

Young's modulus illustrates how a material requires a linear amount of stress to experience a given amount of strain, which varies for differing materials. However, thin films experience biaxial stress due to the two-dimensional nature of the system, where the out-of-plane stress is considered to be negligible. To account for this biaxial scenario, the Poisson's ratio (ν) is used to relate the axial and transverse strains as follows,

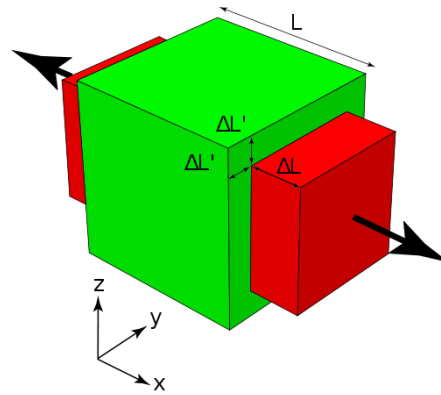
$$\nu = \frac{\epsilon_{\text{transverse}}}{\epsilon_{\text{axial}}} \quad [5]$$


Figure 6: Demonstrating the behavior of the axial and transverse strain of a material while under tensile stress. The initial size and position of the material is represented by a green cube with sides L . While under tensile stress in the x -direction, the material will stretch by a total length ΔL in the x -direction and shrink by $\Delta L'$ in the transverse y and z -directions. The Poisson's ratio is the ratio of transverse strain to the axial strain due to some stress. In this example, $\nu = \frac{\Delta L'}{\Delta L}$. [<http://upload.wikimedia.org/wikipedia/commons/c/ec/PoissonRatio.svg>]

Specifically, as a material experiences a strain due to being under tension or compression in an arbitrary axial direction, the corresponding transverse direction will undergo an opposing strain as seen in Figure 6. This is the material's way of redistributing mass to minimize the internal stresses which would otherwise increase while experiencing an external stress. The total axial strain will accordingly depend on the stress in both axial directions. For a biaxial stress in the x and y dimensions, the corresponding stress may be related by,

$$\epsilon_x = \epsilon_y = \epsilon_{x,y} = \frac{\sigma_x - \nu\sigma_y}{Y} = \sigma_{x,y} \frac{(1 - \nu)}{Y} = \frac{\sigma_{x,y}}{M}, \quad [6]$$

assuming the in-plane stress is uniform ($\sigma_x = \sigma_y = \sigma_{x,y}$) [14]. From this the biaxial modulus may be defined as an effective elastic modulus, altered from the Young's elastic modulus as,

$$M = \frac{\sigma_{x,y}}{\epsilon} = \frac{Y}{1 - \nu}. \quad [7]$$

2.1.3 Thermal Stresses

Stress can occur through various mechanisms. In particular, the stresses that can be reasonably controlled and measured are thermal stresses. Thermal stresses occur through a change in temperature when the coefficients of thermal expansion between the film material and substrate are different. In short, in the case when temperature increases, the expansion of the film material will be different than the expansion of the substrate causing a mismatch stress due to the inability for both the substrate and film to expand together evenly. The simple model of thermal strain for a radially symmetric and uniformly thick thin film with thermal expansion coefficient α_f adhered to a substrate with thermal expansion coefficient α_s under varying temperature ΔT is given by,

$$\varepsilon_m = (\alpha_s - \alpha_f)\Delta T. \quad [8]$$

The mean stress (σ_m) exerted by the thin film then becomes,

$$\sigma_m = \varepsilon_m M_f = M_f(\alpha_s - \alpha_f)\Delta T. \quad [9]$$

This stress can be either radially tensile or compressive depending on the film and substrate materials, or whether temperature is increasing or decreasing. Assuming that the biaxial modulus and substrate or film coefficients of thermal expansion are constant within the temperature range, this demonstrates that the stress will change linearly with temperature. By controlling the temperature of the film and substrate, the stress and strain will be controlled and measured unobtrusively using Houghton College deposition apparatus described in Chapter 3.

2.2 Measuring Stresses

2.2.1 Relating Curvature to Stress

The effects of stress can be measured and the stress can then be calculated using appropriate models. Specifically, stress causes strain to occur to both a thin film and substrate as seen in Figure 7. Since the thin film and substrate are rigidly adhered to each other, the opposing stress they exert on each other will cause them to seek equilibrium through strain which causes them both to bend together as shown in Figure 8. The resulting bending may be characterized by the radius of curvature of the film and substrate system, assuming that the bending is indeed spherical in shape. This is a good assumption to have for thin film and substrate systems where the strain displacement is small relative the actual size of the film and substrate. However, the curvature is not necessarily uniform for every point on the sample, thus there is merit in determining the curvature both locally and non-locally for stress analysis.

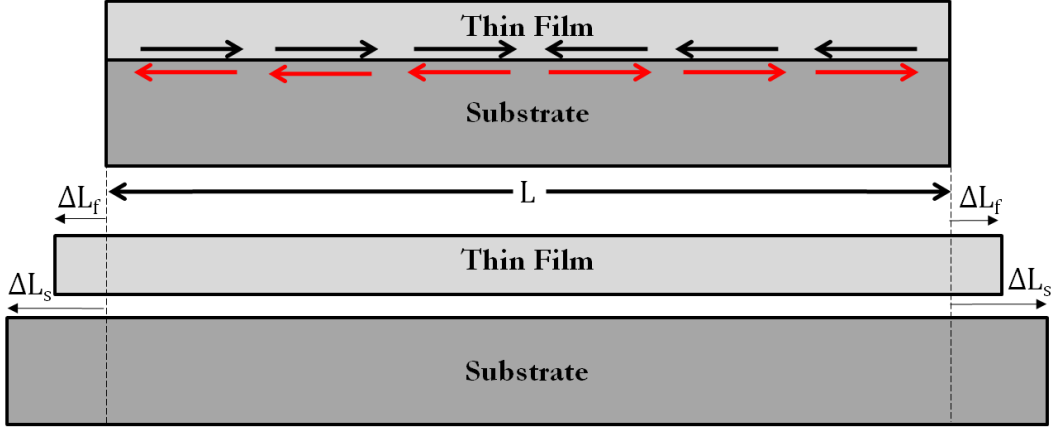


Figure 7: Thin film and substrate initially with length L expand differing amounts in one dimension. The substrate expands ΔL_s whereas the film expands by ΔL_f , thus they experience opposing stresses as represented by the arrows. Since the film and substrate are rigidly adhered together, the varying strains manifest themselves by bending together until reaching a new stress state equilibrium as seen in Figure 8.

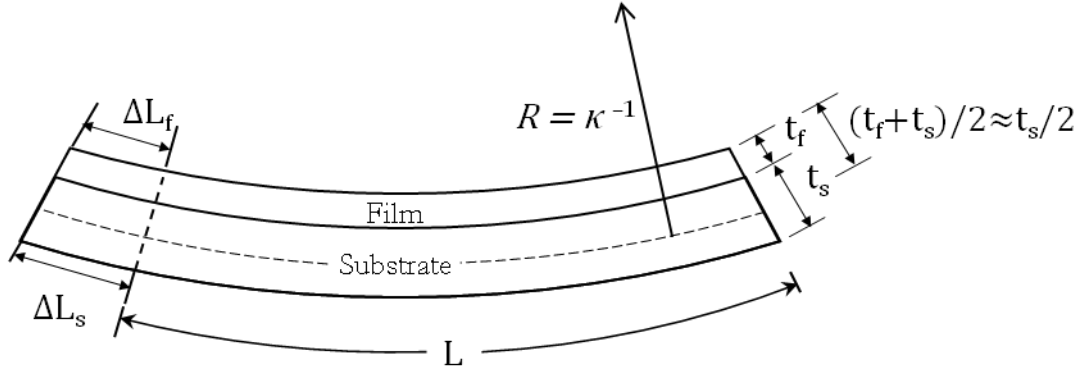


Figure 8: Two-dimensional example of curvature (κ) due to varying strain of a thin film ($\Delta L_f/L$) and substrate ($\frac{\Delta L_s}{L}$). The radius of curvature is measured from the mid-plane of the total thickness of film (t_f) and substrate (t_s).

2.2.2 Stoney formula

Since stress results in a change in film and substrate curvature, the curvature behavior may in turn be modeled to calculate the stress throughout the film. A formula for this may be derived with the implementation of several base assumptions explicitly stated by Freund and Suresh [15] as follows:

- i. Both the film thickness t_f and substrate thickness t_s are uniform, the film and substrate have the same radius ($R_f = R_s$), and $t_f \ll t_s \ll R$;

- ii. The strains and rotations of the plate system are infinitesimal;
- iii. Both the film and substrate are homogeneous, isotropic, and the substrate is linearly elastic;
- iv. The film stress states are in-plane isotropic or equibiaxial (two equal stress components in any two, mutually orthogonal in-plane directions), while the out-of-plane direct stress and all shear stresses (in-plane and out-of-plane) vanish;
- v. The system's curvature components are equibiaxial (two equal direct curvatures) while the twist (shear) curvature vanishes in all directions; and
- vi. All surviving stress and curvature components are spatially constant over the plate system's surface, a situation which is often violated in practice.

In summary, these assumptions each mandate that the curvature has uniform thickness and curvature, which is a good approximation for a thin film/substrate system where $t_f \ll t_s \ll R$. To characterize the curvature of the film and substrate, the strain relative to the mid-plane of the system may be defined by a relation of infinitesimal similar triangles demonstrated in Figure 9. Therefore,

$$\epsilon(z) = \frac{\delta}{a} = \frac{z}{R} = \frac{\sigma(z)}{M_s}, \quad \text{or} \quad \sigma(z) = \frac{z}{R} M_s. \quad [10]$$

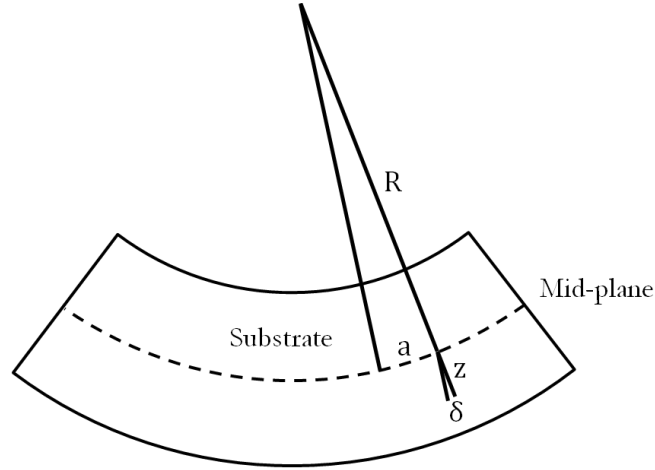


Figure 9: Graphical demonstration of proportionality of $\epsilon(z) = \frac{\delta}{a} = \frac{z}{R}$ by constructing infinitesimal similar triangles. Note that R and z are referenced to the mid-plane of the substrate.

Since the system will be in static equilibrium, the net bending moments will be zero. By letting the moment be about the midpoint axis $z = \frac{t_s + t_f}{2} \approx \frac{t_s}{2}$, the moments for both the substrate and film may be found where the sum will be zero. Since $t_f \ll t_s$, the moment about the film (Ψ_f) will simply be,

$$\Psi_f = \sigma_f t_f \left(\frac{t_s}{2} \right), \quad [11]$$

assuming the film has negligible thickness.

The moment about the substrate (Ψ_s) will need to be integrated across its thickness such that,

$$\Psi_s = \int_{-\frac{t_s}{2}}^{+\frac{t_s}{2}} \sigma(z)zdz = M_s \frac{t_s^3}{12R}, \quad [12]$$

where $\sigma(z)$ is defined in equation 14. Therefore,

$$\Psi_f = -\Psi_s, \quad \text{and} \quad \sigma_f t_f \left(\frac{t_s}{2}\right) = -M_s \frac{t_s^3}{12R}. \quad [13]$$

This yields the Stoney formula,

$$\sigma_f = -\frac{M_s t_s^2}{6t_f R} \quad \text{or} \quad \sigma_f = -\frac{\kappa M_s t_s^2}{6t_f}, \quad [14]$$

with positive being convex on the film face and negative being concave [16]. The total stress experienced by the film (σ_f) is related to the total change in curvature of the film and substrate (κ), biaxial modulus of the substrate (M_s), thickness of the substrate (t_s), and thickness of the film (t_f). Since the substrate and thin film have a thickness, the radius of curvature (R) is defined from the mid-plane of the substrate and thin film as seen in Figure 8. This model shows that an increasing curvature indicates an increasing film stress, which in turn depends on the substrate properties of thickness and biaxial modulus. Also, the measured curvature indicates lesser stress with increasing film thickness, of which a thicker film divides the internal force across the full film thickness, resulting in less stress.

This formula is strictly defined for ideal thin films which follow the criteria outlined earlier in this section, but may be applied for a general understanding of how curvature relates to the stress in a film. For example, the Stoney formula assumes the curvature is perfectly uniform and spherical, which is not always the case. Instead, the mean curvature may be used to determine the mean stress of a film, which would in turn be violating the main assumptions of the Stoney formula. Thus, the Stoney formula must be used circumspectly, keeping in mind that violating any assumption may invalidate the model entirely. However, the model is still useful for determining a basic understanding of film stress by observing the film curvature.

The Stoney formula has been adapted and used in determining thin film stress for many applications, even while not fully abiding by these specific assumptions. In a recent publication by Feng, Huang, and Rosakis summarizing the usage of the Stoney model for non-uniform applications, they state:

Despite the explicitly stated assumptions, the Stoney formula is often arbitrarily applied to cases of practical interest where these assumptions are violated. This is typically done by applying Stoney's formula point-wise and thus extracting a local value of stress from a local measurement of the system curvature. This approach of inferring film stress clearly violates the uniformity assumptions of the analysis and, as such, its accuracy as an approximation is expected to deteriorate as the levels of curvature non-uniformity become more severe [17].

As such the Stoney model has been extended through various adjustments which have worked to relax each of the six assumptions, as well as provide a more general analysis of determining stress from curvature measurements under other varying conditions.

2.2.3 Extensions to Stoney Formula

2.2.3.1 Film thickness on order of substrate thickness

This first extension derived by Brenner and Senderoff [18] addresses the assumption that the film thickness is much smaller than the substrate thickness ($\frac{t_f}{t_s} \ll 1$) and that the elastic moduli of the substrate and film are nearly equal ($\frac{E_f}{E_s} \cong 1$). For arbitrary values of thickness and elastic moduli for both the film and substrate, the following relation was derived to first order of $\frac{t_f}{t_s}$ as,

$$\sigma = \frac{M_s t_s^2 \kappa}{6 t_f} \left[1 + \frac{4 M_f}{M_s} - \frac{t_f}{t_s} \right]. \quad [15]$$

Note that this formula now includes the value for the biaxial elastic modulus of the film (M_s), and the thickness of the film holds a more relevant role in calculating the stress. This formula also effectively simplifies to the Stoney formula, where $\frac{t_f}{t_s} \ll 1$ and $\frac{E_f}{E_s} \cong 1$. Since this formula is only expanded to the first order, its applicability is only suited for small values of $\frac{t_f}{t_s}$. This model may be further expanded to higher orders, but quickly diverges because the curvature behavior changes non-linearly with increasing film stress due to the measured bifurcation present at higher stress.

2.2.3.2 Non-linear Model with Bifurcation

A non-linear stress-curvature relation was first developed by Harper and Wu, shown in Figure 10 with comparison to the Stoney Model [19]. Harper and Wu successfully modeled the behavior of thin films that did not exhibit spherical curvature beyond a critical point of high strain which is observed through

experiments [20]. When the strain exceeds this critical point, the analytical solution for curvature predicts the bifurcation of three equilibrium stress-curvature solutions, two of which are stable and one un-stable. Specifically, the total curvature becomes asymmetric, with the curvature increasing in one direction and decreasing in the orthogonal direction. Under this analysis the curvature is still uniform in magnitude, but merely defines a new non-spherical shape, such as ellipsoid, cylinder, or saddle shape [20]. The analytical solution may be expanded to a form similar to the relation in Eq. [15] through the addition of a correction term that involves more terms using the film and substrate's Poisson ratio, which provides a more accurate stress value for curvature strain near and beyond the bifurcation point [21]. In general this analysis concludes that stress is only mildly applicable to a linear range with low relative strain, and may be further predicted by non-linear means.

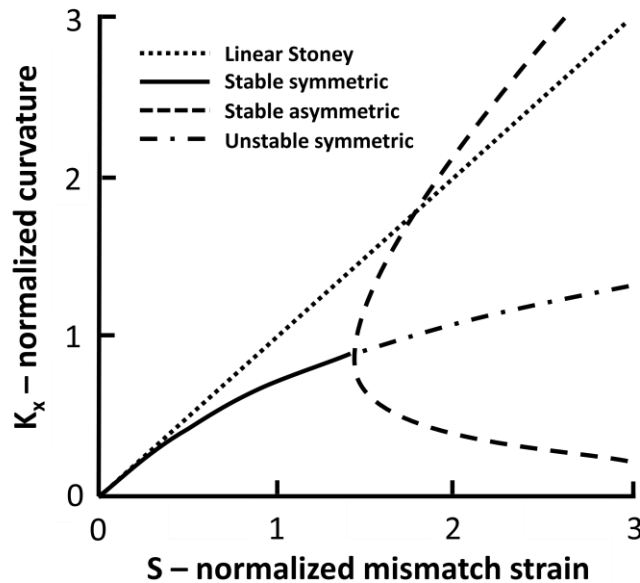


Figure 10: Harper model of curvature due to stress showing bifurcation beyond critical point of $S = 1.43$. The model is normalized to the linear Stoney model, where the strain and curvature are scaled such that $S=K_x$. The linear Stoney model is defined to only be accurate below values of $S = 0.3$. [22]

2.2.3.3 Relaxing assumptions of Stoney Formula

Over the past decade, significant progress has been made in addressing the various uniformity assumptions of the Stoney formula. In 2004, Freund published the derivation for a biaxial form of the Stoney formula which allowed for the accommodation of nonzero in-plane shear stress. This in turn

relaxed the Stoney assumption (v) of curvature equibiaxiality [23]. Further research of bare periodic lines and composite films with periodic line structures allowed for the relaxation of assumptions (iv) and (v) of equibiaxiality and defined three independent curvature and stress components in the form of two, non-equal, direct components and one shear component [24]. The problematic assumption (vi) was finally relaxed by Huang et al. [25] while studying the thin film/substrate system subject to non-uniform, axisymmetric misfit strain (in thin film) and temperature change (in both thin film and substrate), respectively, while Ngo et al. [26] studied the thin film/substrate system subject to arbitrarily non-uniform (e.g., non-axisymmetric) misfit strain and temperature [27]. A valuable discovery from this research is that the film stresses are found to depend non-locally on the substrate curvatures, meaning they depend on curvatures of the entire substrate. From here, Brown et al. relaxed part of the assumption (i) to study the thin film and substrate of different radii, i.e., the thin film has a smaller radius than the substrate, and specifically the stress behavior near the film and substrate edge [28]. Ngo et al. further relaxed the assumption (i) for arbitrarily non-uniform thickness of the thin film [29]. Finally, Feng et al. addressed the remaining portion of assumption (i) by revising the model for the case of non-uniform thickness of the substrate [30]. In each case, the subsequent models are able to degenerate to Stoney's formula when applied to uniform, equibiaxial stresses and curvatures.

Other extensions from the Stoney formula include altering the circular substrate and film shape into a rectangular shape [31]. The Chen group applied the Stoney formula to microelectromechanical systems (MEMS) research and determined the limitations of its usefulness outside its linear range [32]. Non-uniform temperature gradients and its effect on film stress were also explored [33,34]. Other research includes the study of multi-level line structures and the effect of adding passivation capping layers on film stress [35].

2.2.4 Methods for Measuring Curvature

The most straightforward way to measure stress is by indirectly measuring the film and substrate curvature through the use of the models introduced in Section 2.2. Various ways of measuring curvature include mechanical, capacitance, x-ray diffraction, and optical methods, where all but x-ray diffraction measures out-of-plane deflection of curved film-substrate system [36]. The advantage of non-mechanical methods are that measurements are performed in situ, allowing the sample to be unaltered and likely isolated during measurements. Since stress has been found to depend on the non-

local curvature of thin films, there is a strong advantage in measuring the full film curvature in real time through optical methods.

Among optical methods, laser interferometry and laser deflectometry are the most popular. Laser deflectometry, diagrammed in Figure 11, can probe two distinct characteristics of a film, the film curvature and the thickness gradient; however, this technique requires films to be transparent [37].

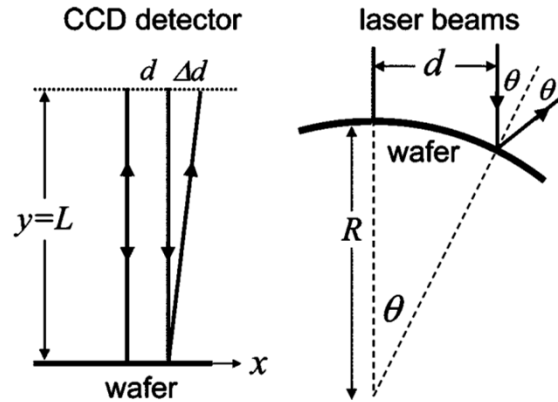


Figure 11: Concept behind laser deflectometry. Two parallel beams separated by d are directed at near-normal incidence on a sample wafer. Light reflected from the wafer is detected with a two-dimensional CCD array detector placed a distance L from the wafer.

The curvature may be extrapolated from the deflected distance Δd [37].

An intriguing interferometry method is the coherent gradient sensing (CGS) technique developed by Rosakis et al. This technique uses a combination of filtering lens and high density gratings to make use of diffraction fringes of laser light incident on a sample which may be recorded and analyzed with software [38]. A diagram and explanation of the setup is found in Figure 12. This technique is also vibrationally insensitive and has been useful in providing experimental data for supporting the recent models developed and described in Section 2.2.

Houghton College is currently developing its own Michelson interferometer for measuring full-film curvature which should be able to provide a topographical curvature map in real time during sample heating experiments.

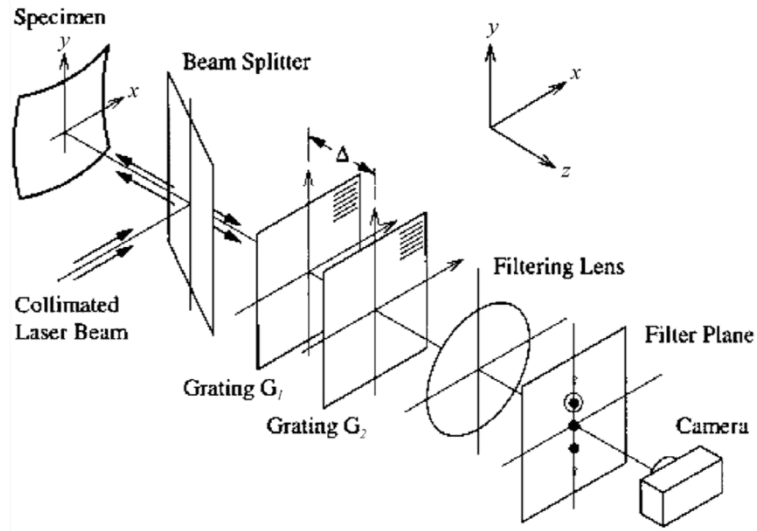


Figure 12: Coherent Grade Sensing (CGS) layout. A coherent, collimated laser beam is directed to the specularly reflecting specimen surface via a beam splitter. The beam reflected from the specimen then passes through the beam splitter and is then incident upon a pair of identical high-density gratings, G_1 and G_2 , separated by a distance, Δ . The diffracted orders from the two gratings are spatially filtered to form distinct diffraction pattern spots on the filter plane. An aperture placed in this plane serves to filter out the diffraction order of interest, which is then imaged onto the photographic film plane. [38]

Chapter 3 : DEPOSITION APPARATUS

3.1 Introduction

The Houghton College deposition chamber project was begun in 2005 and will be ready to begin testing in 2011. The deposition apparatus is used to deposit thin films of a desired composition and thickness gradient, measure the film displacement or curvature of a thin film and/or substrate, as well as control the sample temperature during or after deposition. Components include the vacuum system and pressure gauges, metal evaporation system and deposition rate monitor, sample holder and heater, ion gun, movable shutters, and interferometer apparatus. The chamber and its components will be discussed, with an emphasis on the sample heater and holder, which was the focus of the author's work in the deposition project. A description of the testing procedures is outlined in Appendix A.

3.2 Deposition Apparatus

3.2.1 Purpose

The deposition apparatus will allow Houghton College to deposit thin films of varying thicknesses and materials, and perform experiments while controlling sample temperature to determine film physical properties. This deposition chamber will enable the deposition and analysis of films without ever leaving vacuum, greatly lowering the presence of contamination and increasing convenience by allowing experiments to proceed from start to finish without having to vent the chamber.

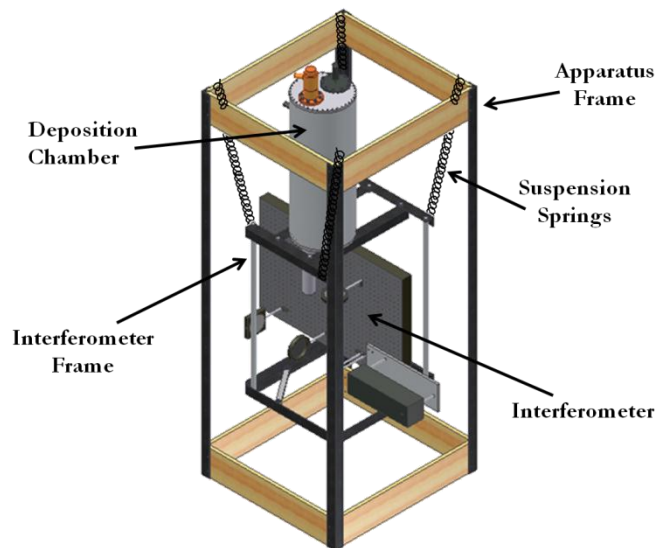


Figure 13: 3D model of chamber and interferometer suspended by springs from the outer apparatus frame to the inner interferometer frame. (Autocad image by J. Mertzluft)

3.2.2 Description

The apparatus is composed of two main parts – the deposition chamber and interferometer, as seen in Figure 13 and Figure 14. The entire apparatus, weighing approximately 100 kg, is suspended in midair by four springs, each with spring constant $k = 812 \text{ Nm}^{-1}$. These springs hang from a rigid outer apparatus frame to a rigid inner interferometer frame, allowing the chamber to be its own vibrationally isolated system. From Hooke's Law, the resonant frequency of this dampening system is,

$$\omega = \sqrt{\frac{k}{m}} = \sqrt{\frac{(4 * 812 \text{ Nm}^{-1})}{100\text{kg}}} \approx 5.73 \text{ Hz.} \quad [16]$$

This resonant frequency (ω) is quite low and is much less than the typical vibrational frequencies of the building, such that higher frequencies will be effectively dampened by the system [39]. Magnets will be placed around the springs to dampen the system further using eddy currents. Eddy current damping is a well-studied method that is common for damping oscillating systems of conducting metals, which causes kinetic energy to be absorbed as electromagnetic energy and dissipated as thermal energy. When conducting materials pass through a magnetic field, an electromagnetic force creates eddy currents which induce a magnetic field to resist the direction of motion, thus damping the velocity and oscillation of the conducting material [39].

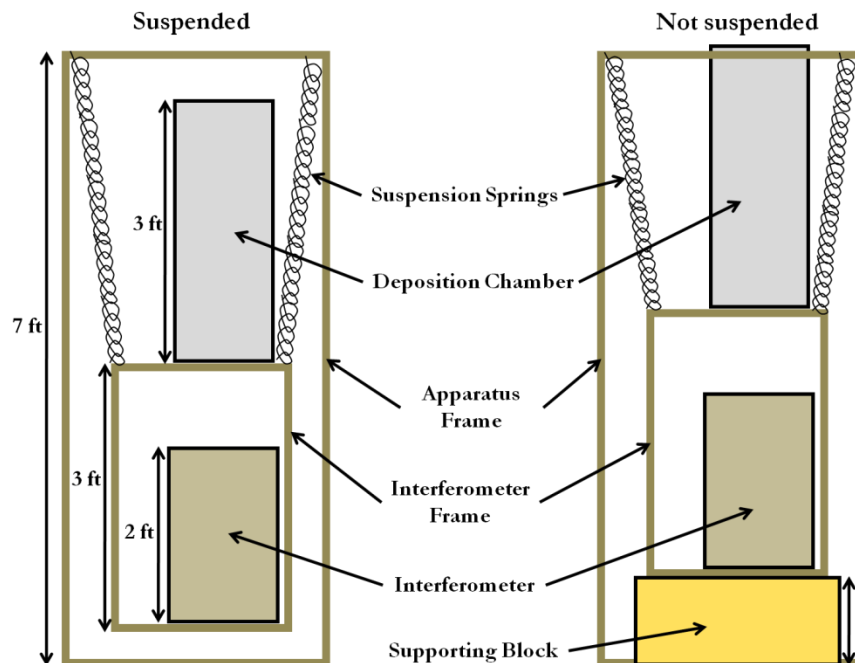


Figure 14: Houghton College Deposition Apparatus suspension system where springs hang the interferometer frame from the apparatus frame. The inner frame may be lifted, allowing a supporting block to be placed below the inner frame to support the system and allow it to sit unsuspended.

The inner frame will utilize a mechanism to pivot and slide the interferometer relative to the chamber for alignment with the sample. The outer frame measures approximately 7 feet tall, the chamber measures 3 feet tall, the interferometer frame measures 3 feet tall, and the interferometer inside measures 2 feet tall. While the apparatus is not being used for deposition or interferometer experiments, the apparatus will be raised and rested on a block designed to support the chamber and enable it to rest in an unsuspended state.

3.2.3 Deposition Vacuum Chamber

The deposition apparatus consists of several components, all of which are needed to make a thin film of a desired composition, thickness gradient, and control the sample's temperature. The deposition vacuum chamber is seen externally in Figure 15 and all of its internal components are diagrammed in Figure 16. This chamber, constructed by Kurt Aikens in 2008, is made from 0.5 inch thick aluminum and is described more explicitly in Kurt Aikens' thesis [40].

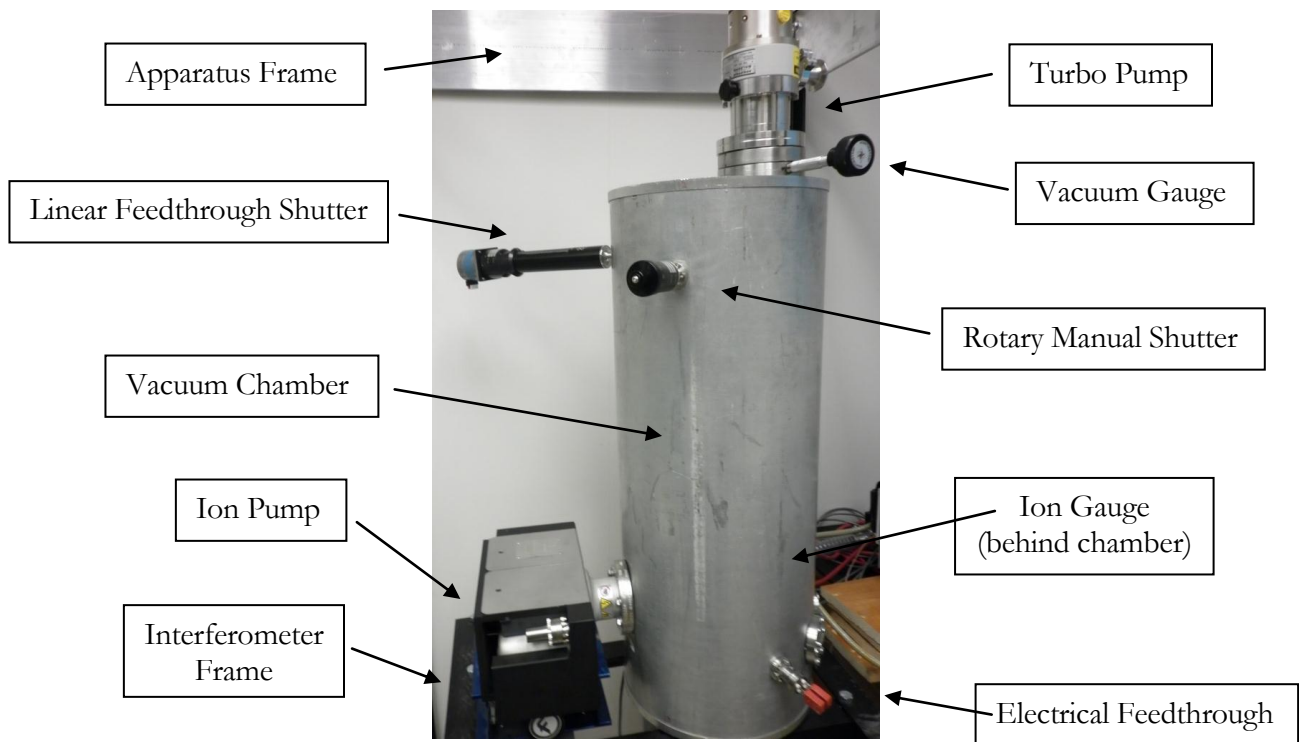


Figure 15: Current external view of deposition chamber with vacuum pump inlets, ion gauge, and electrical and shutter feedthroughs. The deposition vacuum chamber is mounted on the interferometer frame, and within the apparatus frame. The chamber roof containing the rotary feedthrough and sample holder and heater is not shown.

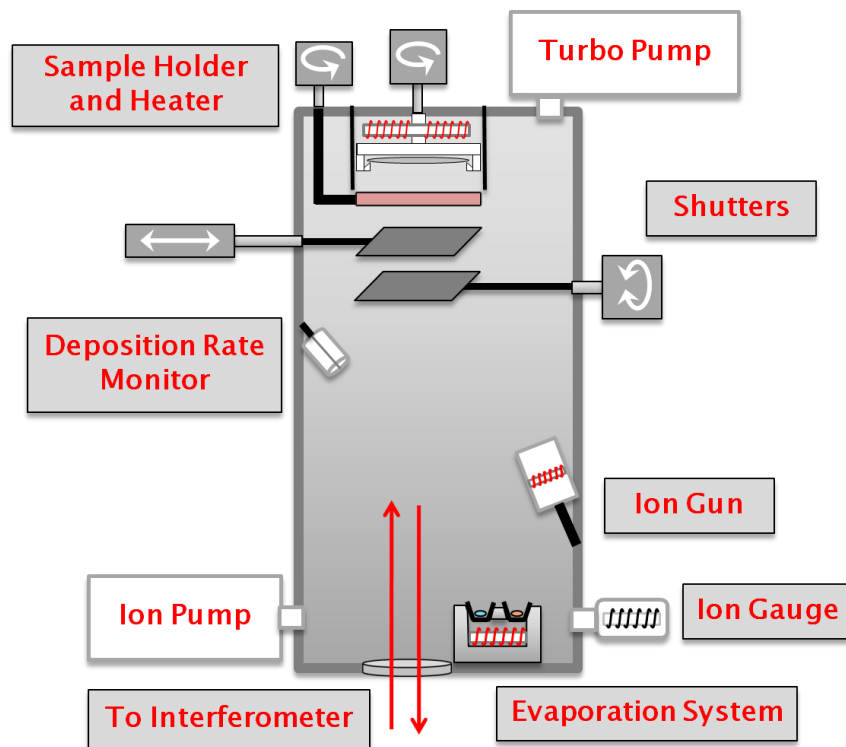


Figure 16: Two dimensional internal diagram of deposition chamber with all components labeled, not to scale. The interferometer emits and receives light represented by red arrows through a glass window in the bottom of the chamber as shown. Note that interferometer beam is directly perpendicular to the sample, with the evaporation system lying slightly offset. The sample holder and heater are attached to the rotary feedthrough fastened to the roof of the chamber, as seen in Figure 17.

3.2.4 Vacuum System

Low pressure is required to reduce sources of contamination for film deposition and analysis; the Houghton College deposition vacuum chamber achieves this by equipping a turbo pump backed by a roughing pump, and an ion pump for maintaining low pressure during experiments. The roughing pump is used to remove the majority of air from the chamber, reducing the pressure to 10^{-3} torr. Once the pressure is within this threshold, the turbo pump is used to lower the pressure down to the 10^{-7} torr level and the pressure is measured by an ion gauge located on the side of the chamber. Due to the mechanical nature of the turbo pump, it is not ideal for use during depositions and experiments, which require vibrational isolation. It is more advantageous to switch over to an ion pump which has no moving parts.

The goal is to achieve pressure as low as 10^{-8} torr which will mostly eliminate the effect of impurities. Contamination will continue to occur over time, but at a negligible rate compared to the time of

deposition. This system is designed to maintain pressure that is at least this low through baking the system for 24 hours prior to deposition. Baking the system involves heating the entire chamber apparatus to over 80°, allowing for residual particles, such as water vapor and other contaminants adhered to the O-ring seals, to more readily degas within the chamber and be removed by the vacuum system. Afterward, the chamber may be cooled to room temperature and residual particles will be even less likely to degas from the chamber walls and internal components.

3.2.5 *Sample Holder and Heater Apparatus*

The sample holder and heater is this author's contribution to the deposition apparatus project. The apparatus was designed and built to work together as one piece in the chamber. The sample holder and heater apparatus is a combined unit which holds the substrate and thin film while it may freely rotate during deposition and heating experiments. It is designed to be removable from the chamber and connect to the electronics necessary for the heating and rotary systems attached. When removed from the chamber, samples 10 cm in diameter may be easily removed, replaced, and secured using the mechanisms described in section 3.3. The sample heater is located above the sample holder, allowing it to heat the non-film side of the substrate using thermionic emission. There are also layers of molybdenum shielding above and surrounding the side of the sample holder and heater. Below the sample, there is a glass infrared shield designed to block and reflect infrared radiation from leaving the sample, while also permitting the light from the interferometer to pass through during heating experiments. This entire system is extensively described in more detail in section 3.3.

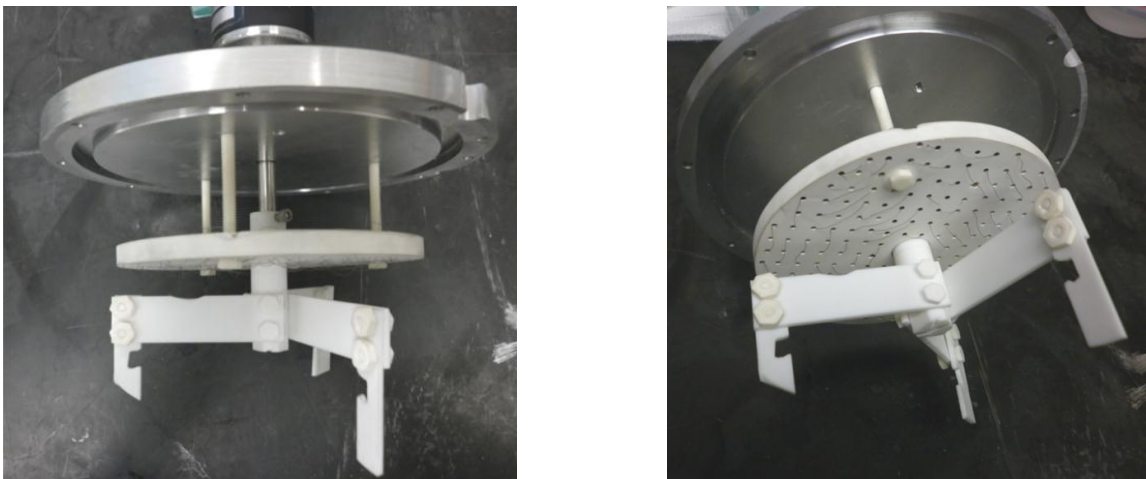


Figure 17 : Images of sample holder and heater apparatus outside of the chamber attached to the removable chamber roof and rotary feedthrough. A sample (not pictured) will set within the prongs of the sample holder tripod as diagrammed in Figure 23 and Figure 24.

3.2.6 Ion Gun

The ion gun is used to clear the substrate surface of atmospheric contamination prior to deposition. It is located on the wall of the chamber as shown in Figure 16, with a diagram shown in Figure 18. A neutral beam of nitrogen ions and electrons are accelerated towards the substrate surface using both magnetic and electric fields, kinematically removing the surface layers of atoms from the substrate. This process may occur with this system by setting the cathode filament current and anode potential, using an external power supply while nitrogen is vented into the chamber at a pressure of ~ 10 mTorr. During deposition, the Ion Beam Assisted Deposition (IBAD) process accelerates ions towards the sample to influence deposited sample density and grain orientation, as well as inhibit sample roughness [40].

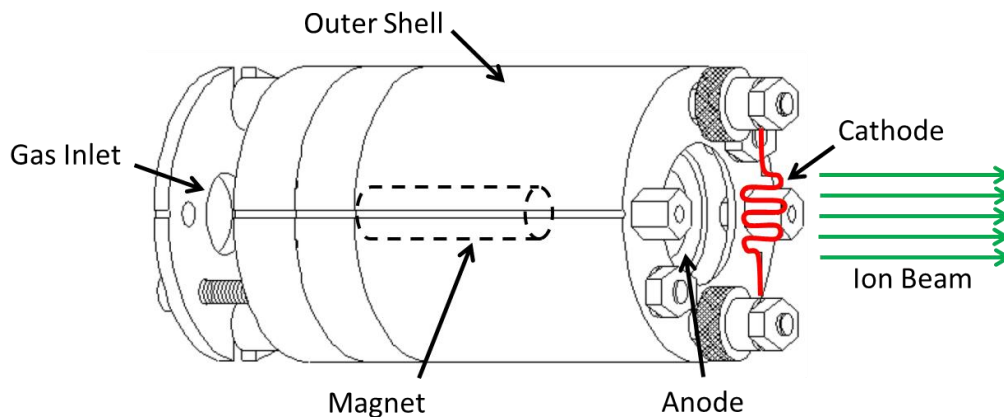


Figure 18: Diagram of gridless ion gun, which ionizes and accelerates gas particles towards the substrate. (Image from Veeco manufacturer user manual)

3.2.7 Evaporation System and Deposition Rate Monitor

Thin films are deposited by the incidence of a flux of evaporated metal on the substrate. Pellets of the target metal are housed in one of four individual graphite crucibles as shown in Figure 19. The metal is heated through thermionic emission by electrons emitted from the respective individual filament under each crucible until it comes to equilibrium at the desired evaporation rate. The current through each filament, and potential difference between each filament and crucible, may be controlled individually by an external power supply. The energy of these electrons will increase the thermal energy of the base of the crucible and be transferred by convection to heat and evaporate the metal placed in the crucible. The intensity of electrons emitted from the filament will determine the equilibrium rate of evaporation for each metal, such that increasing the current through the filament will increase the deposition rate of the film.

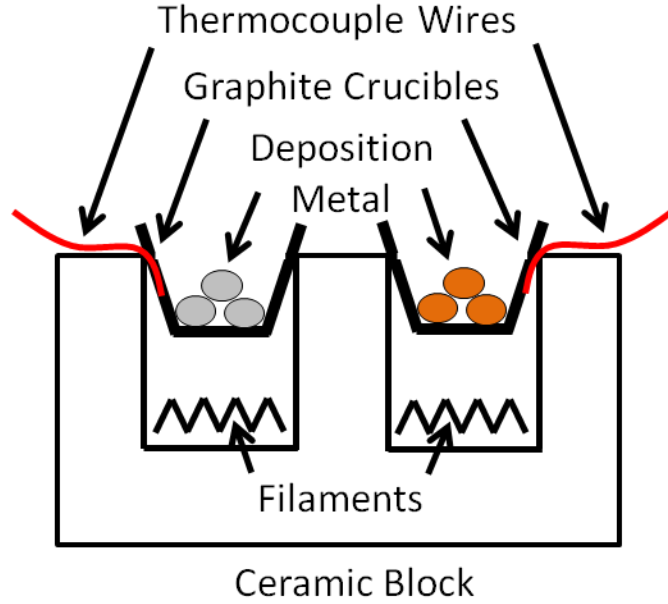


Figure 19: Two-dimensional representation of thermal evaporation system. Pellets of metal are placed in up to four graphite crucibles, each with an independent filament for heating the base of the crucible through thermionic emission. Thermocouple wires are used to monitor the temperature of each crucible during evaporation.

The rate of deposition may be calibrated and monitored using an ion deposition rate monitor placed on the wall of the chamber, oriented toward the evaporation system as seen in Figure 16. The monitor is composed of a molybdenum-anode and tungsten filament-cathode mounted on a 1/8 inch ceramic plate; a diagram is shown in Figure 20. A fraction of the evaporated particles incident upon the monitor will become ionized by accelerating electrons from the filament to the anode held at a higher potential. These ions will in turn accelerate towards the disk-shaped collector at a negative potential, where they will deionize and cause a net current proportional to the rate of ionization. This may be related to the rate of deposition on the sample by,

$$I_{\text{mtr}} \propto \Phi_{\text{mtr}} \propto \Phi_{\text{sbst}} = \frac{t_f}{t}, \quad \text{or} \quad I_{\text{mtr}} = k \left(\frac{t_f}{t} \right), \quad [17]$$

where I_{mtr} represents the rate of ionization measured as current through the cathode, Φ_{mtr} is the rate of particles incident on the monitor, Φ_{sbst} is the rate of particles incident on the substrate, t_f is the thickness of the film, and t is time. Although the deposition rate monitor is not experiencing the same evaporation flux as the substrate near the roof of the chamber, the flux of particles incident on the monitor (Φ_{mtr}) is considered proportional to the flux of particles incident on the substrate (Φ_{sbst}), assuming the evaporation rate is uniform and stable throughout the chamber. Calibration of this

proportionality constant (k) may be determined by depositing a test film at constant evaporation rate current and comparing the actual thickness of the film (t_f) with respect to the time of deposition (t).

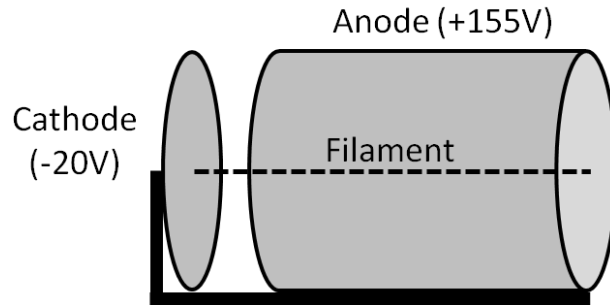


Figure 20: Deposition rate monitor, which ionizes incident particles with the anode and collects the ionized charge as current at the cathode.

Due to the thermal nature of the deposition, the evaporation system will need to be increased gradually to ensure a stable and uniform deposition. Deposition to the substrate may only commence when the deposition rate reaches a stable level, while also ensuring that metal does not run out as it evaporates from the crucible. Metal target pellets may be added to replenish the crucibles while the chamber is vented by removing the window in the base of the chamber and reaching up into the chamber, or by lowering pellets through the roof of the chamber.

3.2.8 Shutters

In order to restrict and control deposition onto the substrate, several moveable shutters may be used to cover the sample before, after, and during depositions or heating experiments. A manual rotary shutter located directly below the sample may be rotated to completely cover or expose the sample to the evaporation system or ion gun; this enables instantaneous control for beginning and ending deposition or ion cleaning. While the shutter is open, the sample is exposed, and by rotating the shutter 90 degrees, the entire sample will be covered. A linear feedthrough shutter is also located directly below the sample, and directly above the rotary shutter. This linear feedthrough shutter has a horizontal range of 4 inches, which may be accurately controlled using a programmable motor, allowing for uniform depositions with thickness gradients. When fully extended, the linear shutter may completely cover the sample, and when the shutter is fully retracted the sample will be fully exposed. In general, shutters must be moved to various specific positions depending on the impending process, such as pre-deposition, mid-deposition, post-deposition, and interferometer experiments.

3.2.9 Interferometer

The Houghton College Interferometer design is shown in Figure 21. The entire interferometer is mounted to a stand which is fastened to the inner frame of the deposition apparatus as shown in Figure 13. A 25 mW laser is diverged using a lens with focal length of 6 mm and passed through a beam splitter to create two paths for the light to follow. When each diverged beam is 4 inches in diameter, it is collimated using a lens with focal length of 18 cm. One beam passes through the window in the bottom of the chamber, the glass infrared heat shield, and is then reflected 180° by the sample such that it returns back toward the interferometer. The other beam is reflected by a piezo-electric ceramic controlled reference mirror, which oscillates to create a controlled path length difference between the two beams. Each beam returns to the beam splitter, creating a superimposed beam which is projected onto a screen within the interferometer. A CCD camera will record the resulting diffraction pattern produced by the two beams in real time into a computer.

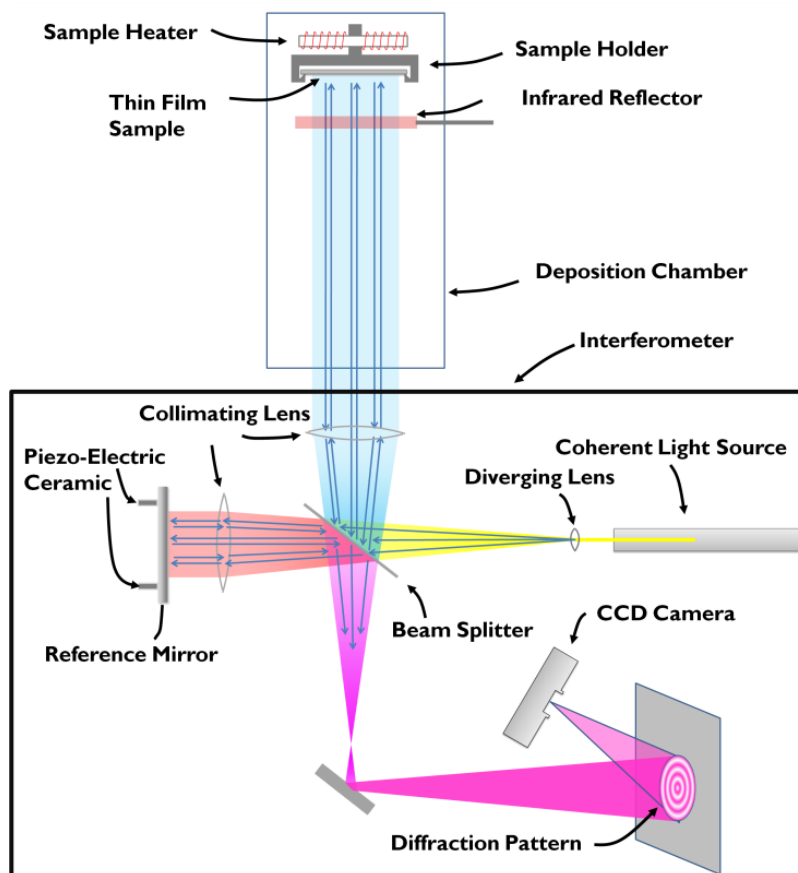


Figure 21 : Diagram of laser interferometer and deposition chamber. A CCD camera records the diffraction pattern from the superposition of two beam paths to measure the film and substrate curvature in real time while placed inside the deposition chamber as shown.

A reference mirror is attached to a rigid mount with piezo-electric ceramic to cause the mirror to oscillate in the transverse direction at a controlled sawtooth-wave frequency with period $T = 1/f$ and amplitude on the order of micrometers in order to change the phase of one beam by at least one full wavelength. The resulting images from the diffraction pattern are recorded by the webcam at a sample rate of 0.5 Hz, providing $T/2$ images per period of oscillation T . These images are stored and used by a computer to calculate the relative phase shift of each pixel of the sample for each period of oscillation. For each pixel, the resulting phase shifts for every time interval T are compared and the change between each phase shift represents a change in path length relative to the reference plane. Once all of the path lengths for each pixel are calculated, the result is a two-dimensional spatial array which provides a topographical map of the sample relative to the reference plane; this may in turn be used to determine the curvature of the sample. The actual thickness of the sample is not necessary to determine the curvature because the curvature needed for stress calculations is determined by the relative change between the initial position of the sample and the final position of the sample, which has been determined by this method.

Once the interferometer is mounted to the inner interferometer frame, it must be aligned to be perpendicular with the sample within the chamber. While mounted, the interferometer must be allowed three translational degrees of freedom and the ability to be secured at the final position once perfectly aligned with the sample. The interferometer will be aligned to the sample by physically moving, pivoting, and sliding the interferometer until both reflected beams of light from the sample and reference mirror are parallel and occupy the same position. Ideally, an accuracy of $1/100^{\text{th}}$ of one inch is suitable, which represents the size of one pixel measured by the camera.

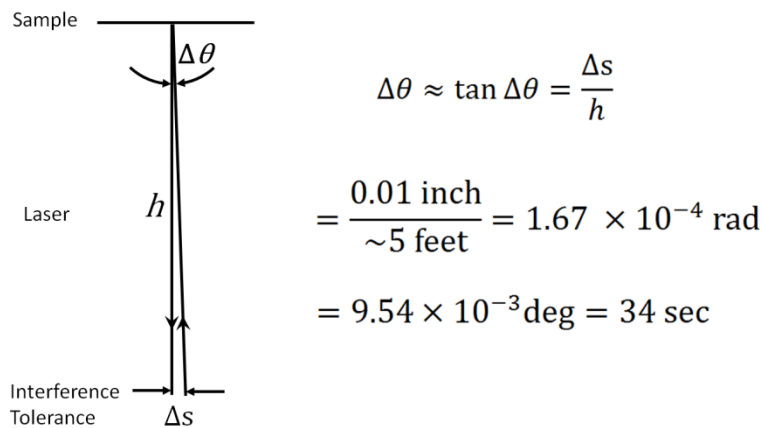


Figure 22: Interference precision required to be stable for CCD pixel measurements of the interferometer.

Figure 22 demonstrates that to attain this accuracy, the perpendicular angle between the sample and interferometer must be stable to the order of seconds of a degree, in addition to the position to being stable to hundredths of one inch; this is assuming the path length is on the order of 10 feet between the point of incidence and point of detection by the camera. While this level of precision is required for the interferometer, it is also required of the actual sample holder which is described in the next section. However if the system is vibrationally stable, any initial misalignment that exists and remains constant will be able to be corrected by subtracting the initial diffraction pattern from all of the measured results, therefore providing a reference curvature which may be initially arbitrary. The system is optimized for measuring the change in curvature, meaning there may be no practical way to determine the actual curvature or thickness of the film. However, since film stress may be readily measured through a change in curvature due to changing temperature, the initial curvature value is unnecessary for the calculation of the changing stress causing the changing curvature.

3.3 Sample Holder and Heater

3.3.1 Sample Holder

The sample holder is constructed with several Macor machine-able ceramic pieces fastened together with ceramic screws and nuts, allowing for total disassembly or removal of the sample. A ceramic rod is fastened to a rotary feedthrough attached to the removable roof of the chamber using a set screw, and the three legs of the sample holder are fastened to the rod, as seen in Figure 23.

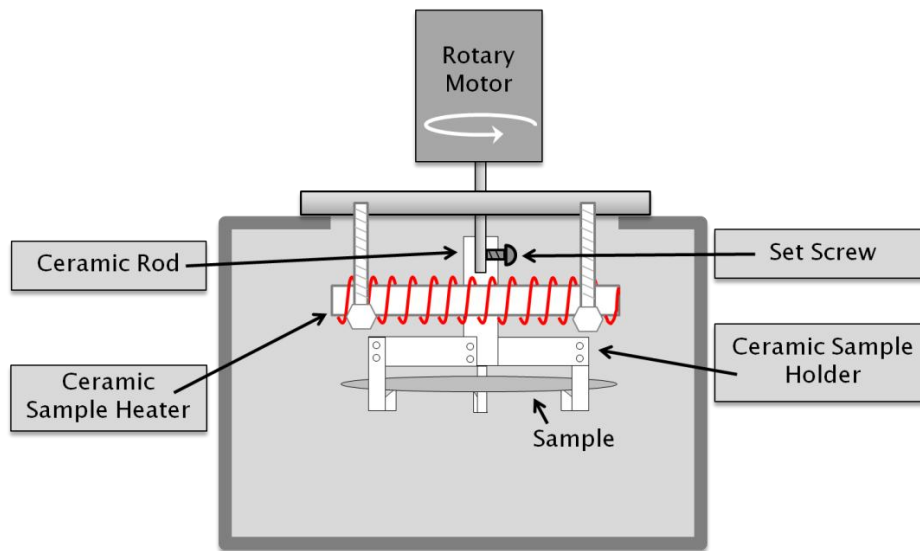


Figure 23: Diagram of sample holder and heater while attached to the roof of the chamber. Both are machined from thermally insulative ceramic, with the sample heater being held to the removable deposition chamber roof by a set of ceramic screws and the sample holder being held to the rotary feedthrough rod with a set screw.

The holder is designed to allow the sample to rest on the tips of the legs of a tripod, which will determine the plane of the sample relative to the chamber and interferometer. The three tips must be aligned to allow the sample to set perpendicular to the axis of the rotary feedthrough, of which the sample holder is attached, so that the plane of the sample does not change as it is rotated. Also, the substrate is allowed to rest on the three tips of the holder without any other forces acting on it in order to allow the sample to be free from stress in any other directions. Since the sample holder is fastened to a rotary feedthrough, samples may rotate for uniform cleaning during ion gun treatment and uniform depositions.

3.3.1.1 Sample Holder Design Choices

The sample holder is constructed out of Macor ceramic to resist the thermal effects due to the nearby heater apparatus. Ceramic is a thermal insulator, having a thermal conductivity of $1.46 \text{ W/m}^\circ\text{C}$ at 25°C , meaning that thermal energy conducts slowly through the material. The advantage of constructing the sample holder entirely out of ceramic is that the effects of thermal expansion will be balanced throughout the sample holder; if the sample holder contained other materials, thermal expansion may cause undesired effects in the dimensions, structural integrity, and especially alignment or tilt of the sample holder. Macor ceramic's melting point is 982°C , which ensures that the sample holder will be suitably rigid and dependable during heating experiments.

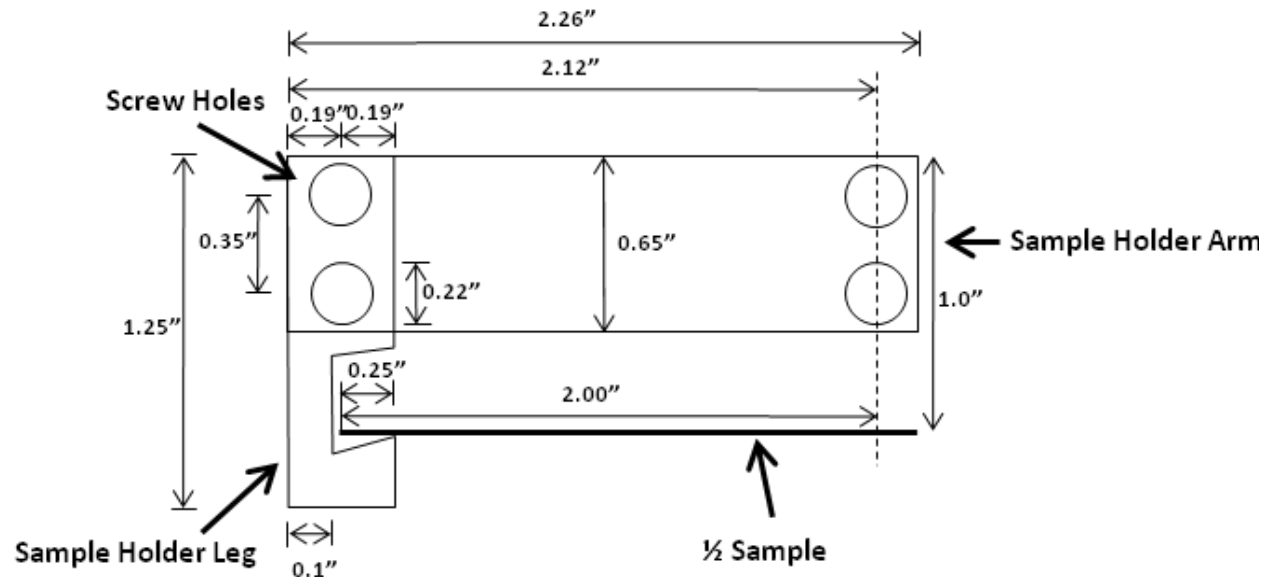


Figure 24: Dimensions of sample holder components, drawn to scale. Note that the diagram is a radial cross-section, thus only showing half of the sample.

The dimensions of the ceramic pieces are diagrammed in Figure 24. The particular dimensions were machined to the nearest hundredth of an inch to accommodate the restrictive limitations of the sample size and hole in the chamber ceiling which have comparable dimensions as seen in Figure 25. The substrate radius is 2 inches and the radius of the hole in the roof of the chamber is 2.2 inches, meaning the radius of the sample hole may only be marginally smaller than the hole while large enough to fit around a sample. A radius of 2.14 inches was chosen to be a suitable dimension for the sample holder, providing a reasonable thickness of 0.1 inches for the vertical ceramic leg to support the sample.

Each piece is made from a ceramic plate 0.7 inches thick, and they are all fastened together using 6-32 ceramic screws and nuts as seen in Figure 17. Because the ceramic nuts have a diameter of almost 0.35 inches, each pair of ceramic screw holes must be separated by that amount in order for each corresponding nut to turn freely and independently. Fortunately, the necessary holes to be drilled into the ceramic were only 0.22 inches in diameter, which is the diameter of the 6-32 screw itself. The screw holes determined the horizontal piece to be 0.65 inches tall, marginally containing the screw holes themselves. The screw holes are not tapped because of how thin the ceramic pieces are. However, the ceramic rod does have tapped holes which allow the screws to fasten directly to it.

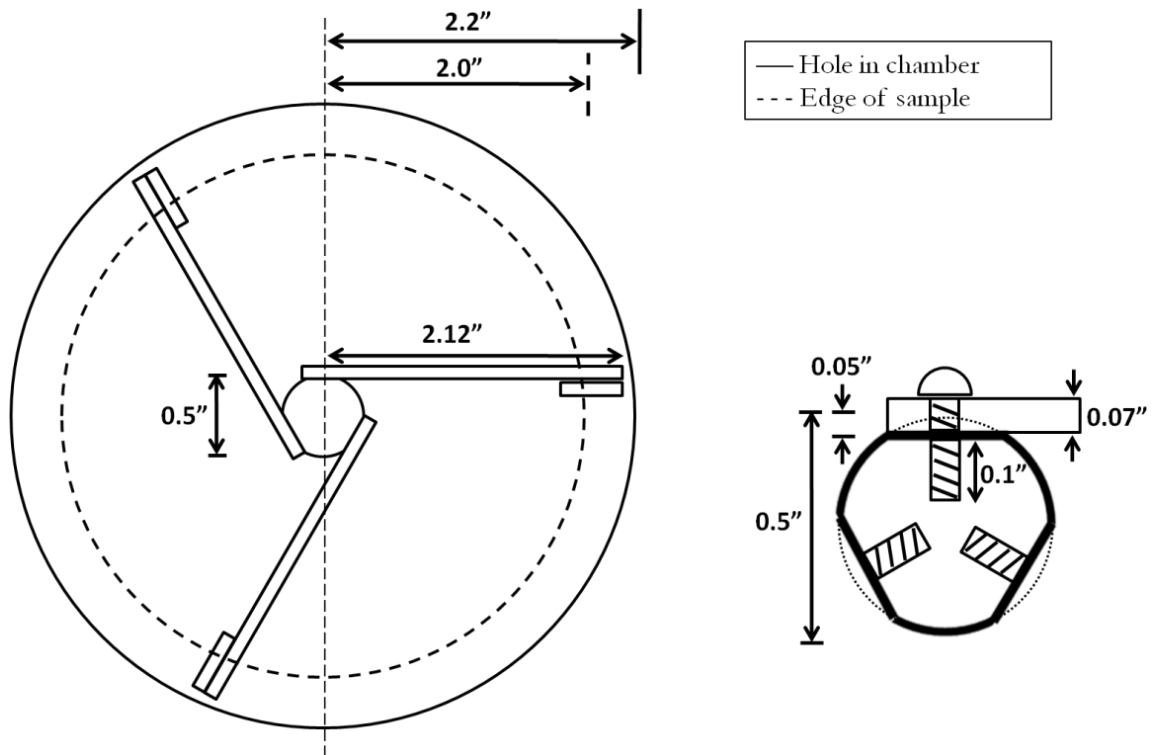


Figure 25: Top down view of sample holder with dimensions of sample, sample holder, and hole in chamber ceiling.

Each of the three legs of the sample holder were made identical and attached to a ceramic rod with 0.05 inch notches every 120° as shown in Figure 25. The 6-32 ceramic screws were shaved to a length of 0.17 inches in order to not collide with each other in the center of the ceramic rod. The alignment of the screw holes is very important for keeping the sample perpendicular to the rotation axis; a slight misalignment of the screw holes will yield a relatively large displacement of the sample while it rotates. This can be corrected by aligning the tips of the sample holder independently of the misaligned legs. Since each of the three legs, tips, and screw holes are slightly different, it is necessary to keep each piece marked and kept to its corresponding position; even though the stage arms are mostly identical, interchanging them will lead to severe and inconsistent misalignment. Once the tips of the sample holder are fully aligned, all of the pieces must stay in their current position, only to be removed and replaced precisely where they were originally situated.

3.3.2 *Sample Heater*

The sample heater is a circular 0.25 inch thick ceramic plate with a diameter of 3.9 inches which has been milled to have over one hundred holes for tungsten wire to thread through as shown in Figure 26. Unlike the sample holder, the heater is held rigid to the chamber ceiling by 1.5 inch ceramic screws. The ceramic heater also contains a 0.5 inch hole in the center, which is where the ceramic rod of the sample holder will fit through. The filament of the heater is tungsten wire that is fed through a circular array of over one hundred holes as seen in Figure 26.

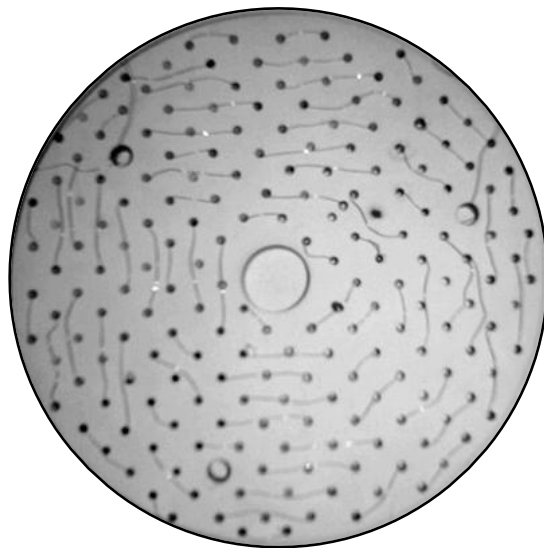


Figure 26: Sample heater with tungsten wire threaded in circular pattern throughout the ceramic plate. The wire ends are threaded through the screw holes to an external power supply.

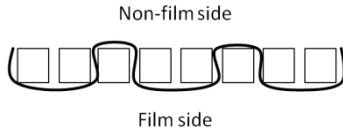


Figure 27: Side view of one interweaving pattern used for wiring the tungsten filament for the sample heater. The wire is threaded to maximize the amount of wire exposed to the film side, which is enhanced by skipping holes and allowing for more wire to be on the film side. The actual heater is wired uniquely, but follows this pattern as a general guideline.

Specifically, the wire is interweaved through the holes in one side of the heater and out the other side of the heater, as demonstrated in Figure 27; not all of the holes were necessarily used in this current wire configuration; this reduces the total length of the wire and increases the amount of wire exposed to heat the sample. An ideal wiring configuration would be uniformly distributed throughout the heater and minimize the amount of wire that is wasted on the opposite side of the sample. Reducing the length of the wire would reduce the voltage needed to heat the sample while increasing the amount of wire exposed to the sample, thereby reducing the current necessary to heat the sample.

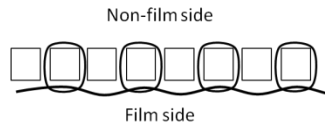


Figure 28: Alternate tungsten wire weaving pattern for maximizing ratio of heater wire on film side of ceramic heater.

Figure 28 demonstrates another wiring configuration which would allow maximum usage of the wire to heat the sample. The heating wire would be suspended by loops of wire on the sample side of the heater, essentially eliminating any unused wire for heating the sample which occurs in the previous configuration in Figure 27. This method may heat the sample more efficiently than the other configurations, but it would require inserting many loops into the ceramic and may not be worth the effort. The disadvantage of wiring the sample heater is due to the great length of the wire that needs to be threaded, where it becomes increasingly difficult thread each successive hole without breaking the wire. As of this writing, the wire has two breaks in the middle of the heater which were spot-welded back together, and no problems occurred during initial testing. If the tungsten wire experiences another break, an alternate wiring method or more careful wiring would help avoid future problems. There are a few holes which contain permanently embedded drill bits, and hence cannot be used for threading the wire; it is expected that the residing material will not cause any issues with heating experiments, but is something to monitor during testing.

The orientation of the wiring is close to uniformly distributed throughout the heater, and roughly radially symmetric about the sample. The current chosen configuration is seen in Figure 26, and generally follows a rotationally symmetric pattern about the center. It was more convenient to drill the holes in a rectangular grid rather than a cylindrical grid, so the resulting pattern is not perfectly symmetric. To improve the uniformity of heating the sample, the distance between the wires should be minimized and symmetric, as well as increasing the distance from the heater to the sample. The current wiring configuration and distance to sample should be suitably uniform, and will be confirmed or refuted through testing. Regardless, since the heating is intended to occur slowly, any temperature gradients occurring in the sample should be minimal and as such the sample should essentially heat uniformly. The sample may have a radially symmetric temperature gradient, but will hopefully be uniform enough to make temperature measurements accurate to the nearest degree Celsius. Although thermionic emission will contribute to heating the sample, the expected dominant mechanism of heating the sample will be through radiant heating by the filament.

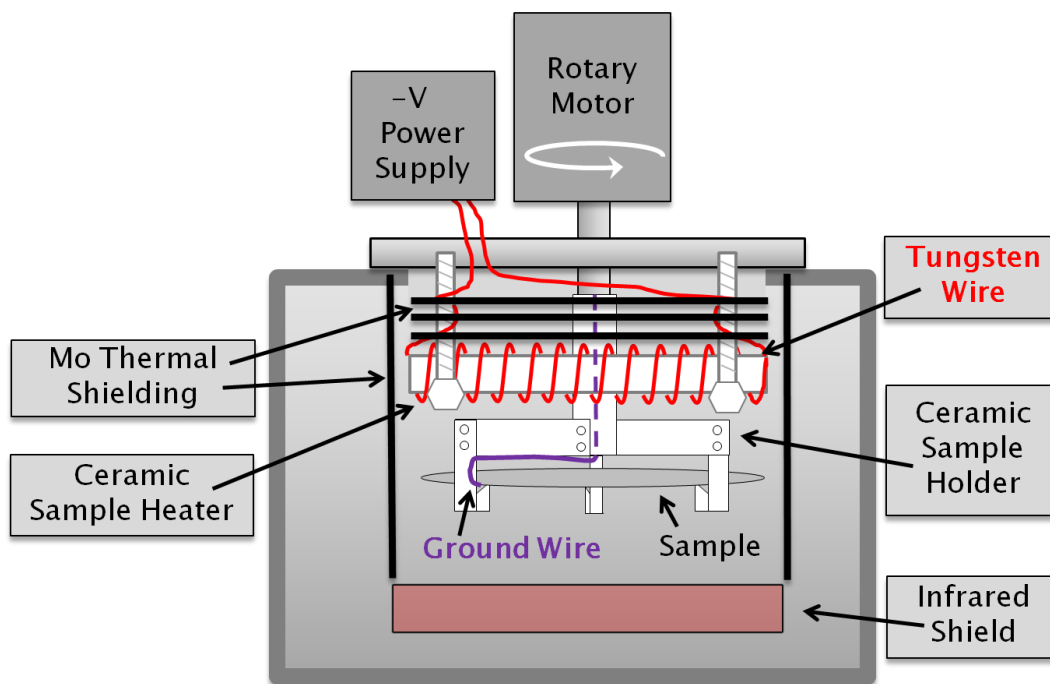


Figure 29 : Sample holder and heater with shielding and electronics. A wire holds the sample at ground, while the tungsten wire is held at a floating potential, contributing heating by thermionic emission. The infrared heat shield reflects radiation from the underside of the sample, keeping the sample thermally isolated, while allowing for interferometer measurements.

The tungsten filament wire will be held at a floating negative voltage of several hundred volts, with a small potential difference across the wire itself to emit electrons for heating the sample with thermionic emission. The wire will be connected through a feedthrough in the roof of the chamber, as seen in Figure 29 and Figure 30. The sample is held at a ground potential through the use of a ground wire applied with silver paint near the tip of one of the sample stage's arms; this ground wire is connected to the chamber by being fed along the stage's arms up into the aluminum feed through rod attached to the stage. Grounding the sample will allow electrons from the heater to be uniformly accelerated by thermionic emission during heating by the potential difference between the heater and sample.

During heating experiments, the sample temperature may be controlled by the sample heater and indirectly measured by the temperature of the molybdenum shielding surrounding the sample. Ideally, the temperature should be measured through direct contact of the sample; however it is not practical to affix a thermal couple directly to the sample, both for the inconvenience of affixing the thermal couple to each individual sample, and for the detrimental effect of adding an extra point of contact to the sample for interferometer experiments. Instead, the temperature will be measured indirectly and calibrated to the sample by comparing the actual temperature of a test sample with the measured temperature of the surrounding molybdenum shielding.

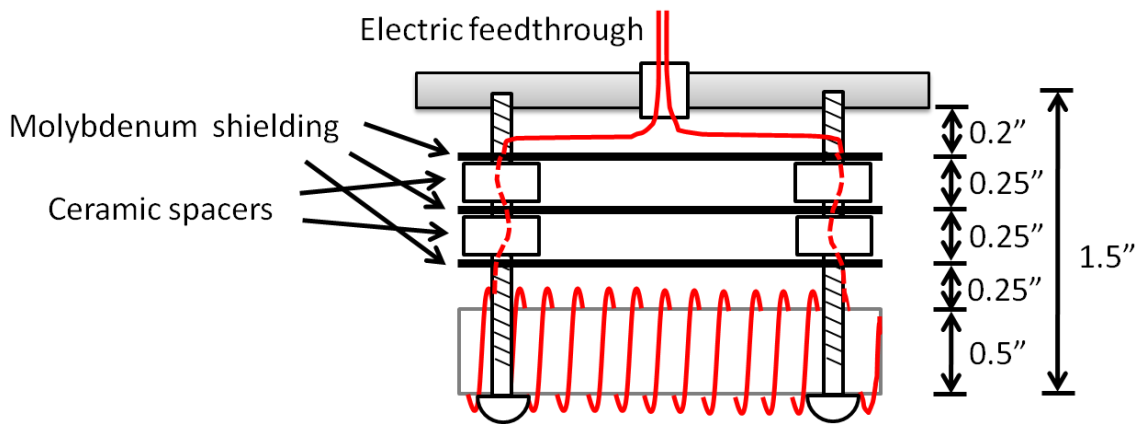


Figure 30: Close up of sample heater and molybdenum shielding with dimensions. Shielding is separated by ceramic spacers along the ceramic screws as shown. The wire for the heater also follows along two separate ceramic screws, where they connect outside the chamber through an electrical feedthrough.

3.3.3 Thermal Insulative Shielding

Ceramic has been used extensively for its use as a thermal insulator, and it serves as the components for all pieces in most direct contact with the sample heater. Molybdenum is a thermally conductive metal with a melting point of 2896 K and low coefficient of thermal expansion and high thermal conductivity. This allows molybdenum to quickly disperse heat and provide a uniformly thermal environment for heating a sample.

Since the heater will radiate heat throughout the chamber, several 0.5 mm sheets of molybdenum are placed above the heater apparatus and around the side of the sample holder and heater as seen in Figure 29 and Figure 30. Three layers of molybdenum are spaced 0.25 inches apart using a ceramic spacer, with the heater wire fed along the 1.5 inch ceramic screw and through a feedthrough in the roof of the removable chamber ceiling. The concept behind using several sheets of molybdenum at separated distances is to enhance the dissipation of thermal energy from the heater into the chamber by gradually absorbing thermal energy and radiating through vacuum to the next molybdenum sheet providing a more gradual temperature gradient from the heater to the chamber. The cylindrical molybdenum sheet surrounding the sides of the sample and heater will aid in thermally isolating the system, limiting the heat to escape the system before reaching the sample. The cylindrical sheet sets within 0.5 inches from the sample holder and heater apparatus, making it close in proximity to the sample and heater, effectively channeling the thermal energy down to the sample.

Below the sample, the glass infrared heat mirror is placed on a rotary feedthrough which will block and reflect outgoing infrared radiation escaping below the sample during heating experiments. The glass is mounted such that it can be removed or replaced within the chamber by setting into an aluminum frame. During deposition, the heat shield may be pivoted to be covered and protected by another molybdenum sheet, keeping it safe from deposition contaminating its surface. There is concern that the heat shield may expand non-uniformly while under a temperature gradient, causing undesired refraction for the interferometer measurements. This has been addressed by affixing the heat shield to its aluminum support holder with ceramic screws.

Chapter 4 : FUTURE EXPERIMENTS AND CONSIDERATIONS

4.1 Current Status - 2011

The Houghton College deposition apparatus is nearing completion as components are being constructed and tested for their functionality. The aluminum deposition vacuum chamber, ion gun, ceramic sample chamber and heater, evaporation system, deposition rate monitor, interferometer, interferometer frame, and apparatus frame have all been constructed by summer 2011. The deposition chamber has been mounted to the interferometer frame, and springs have been installed to suspend it with the apparatus frame. Molybdenum shielding has also been installed in the deposition chamber surrounding the position of the sample holder and heater. The infrared heat mirror has been mounted to the chamber and the electrical feed-through for the heater has been installed. The sample heater has been tested for functionality and successfully heated a blank substrate by 50°C while under vacuum in the deposition chamber. The vacuum chamber and ion gauge have been tested to determine the system's vacuum pressure capabilities, but the other remaining components have only been installed and not yet tested.

The interferometer apparatus has been constructed and its components have been put into place. Piezo-electric control of the oscillating reference mirror is operational and a distinct and measurable diffraction pattern may be seen while using a blank substrate as the testing sample. The diffraction image enlarges with longer path length, so a mirror is added to redirect the image to a corner in the interferometer where it may be projected and measured by a CCD camera as shown in Figure 31. Concerns have been raised for the system's ability to absorb and disperse heat from within the chamber. Even with the heat mirror in place, the glass window at the bottom of the chamber seemed to absorb an excessive amount of heat non-uniformly, meaning the refractive properties of the glass may cause inconsistencies with the interferometer diffraction images.

4.2 Future Goals

At Houghton College, there are still various phases of the project that need to be completed before a straightforward thin film deposition and stress analysis can occur. Further testing of the ion gun, sample heater, evaporation system, deposition rate monitor, and shutter systems will continue after summer 2011.

The interferometer still needs to be mounted to the interferometer frame and aligned to the sample holder in the deposition chamber; this mounting system will allow for three rotational degrees of freedom for the interferometer apparatus so it may be initially aligned to the sample holder in the deposition chamber. Interferometer software is still in development and needs to be tested; this includes importing images from the CCD camera, processing each image and determining the phase shifts for each respective pixel, generating an array of values for a topographical map of the sample, and finally determining the curvature and stress for each experiment.

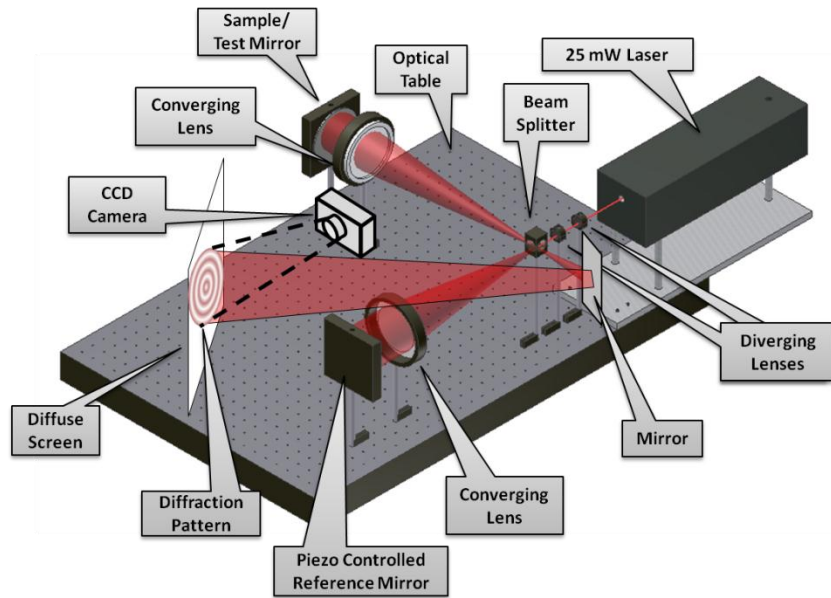


Figure 31: Proposed interferometer apparatus diagram with laser path highlighted in red. The image will be redirected by a mirror to be projected onto a screen and recorded by a camera. (Autocad image by Joshua Mertzluft)

The evaporation system and deposition rate monitor must also be tested and calibrated while under vacuum, after which the system may be used to deposit thin films using the sample holder and shutter systems. The motor for the sample holder rotary feed-through and the controls for the sample heater, evaporation system, ion gun, and linear shutter still need to be set up. Gauges for the deposition rate monitor and thermal couples also need to be installed.

Ultimately, the end goal for this project will be to deposit thin films with controllable thickness gradients, layers, and sample temperature, measure the sample curvature in real time during heating cycles while under vacuum, and analyze the curvature to determine and verify the film stress using the appropriate models. With more effort, this system will be fully functional within several years.

Appendix A : EXPERIMENTAL PROCEDURE

A.1 Goals for Deposition Experiments

With the Houghton College deposition system, thin films may be fabricated and tested for their microstructure properties and behavior under varying conditions of film material, film thickness, and film temperature all while under vacuum with a single integrated apparatus. Thin films may now be studied locally at Houghton without fully relying on other institutions for instruments, such as has been the tradition by collaboration with Cornell University. Once the construction and testing of the deposition apparatus is completed, films may be deposited and analyzed with the interferometer, x-ray diffractometer, and scanning electron microscope in Houghton over the course of each school year. Films may then be brought to other institutions during the summer, such as Cornell University, and be tested with other instruments, such as electron backscattering and focused ion-beam imaging, for determining other film properties and verifying the accuracy of the instruments used at Houghton. As the Houghton College Physics Department acquires and troubleshoots more instruments, the opportunities for thin film research will increase significantly with each new working device.

A.2 Preparing for Deposition

Prior to any deposition or experiment, the system must be appropriately prepared for the tasks that are to be performed.

If depositing a thin film, the crucibles must be filled with enough material for the desired process; the appropriate amount will depend on the planned deposition rate and duration, as well as the pre-deposition routine for allowing the deposition to reach an equilibrium steady state.

A.2.1 Placing Substrate into Sample Chamber

The substrate must be placed in sample chamber and heater apparatus with the polished side facing away from the heater. The substrate may be inserted by removing one ceramic bolt from one of the ceramic legs of the sample holder, placing the substrate within the holding area of the sample holder tripod, then replacing the bolt. The sample holder and heater apparatus may then be carefully lowered into the hole in the roof of the chamber and cylinder of molybdenum shielding. The radial span of the sample holder and heater is only marginally smaller than the size of the hole, so care must be taken to not bump any of the fragile ceramic pieces while lowering into the chamber. The detachable roof of the chamber will then be secured to the body of the chamber by fastening the screws and sealing the

top O-ring. Next, the rotary motor and electric feedthrough for the sample heater may be connected to each of its respective power supplies. If necessary, the angular position of the sample may be noted for future reference. In general, the manual rotary shutter and linear feedthrough shutter will also be aligned to cover the underside of the substrate; the infrared heat shield will be rotated and tucked behind a shield, only to be moved in front of the sample during interferometer experiments. Now the system is ready to go under vacuum.

A.2.2 Bringing System to Vacuum

Once the chamber is sealed and all pump-down preparations have been made, the system may be evacuated starting with a roughing pump, which is in-line and backing a turbo pump. Once the pressure is reduced to the millitorr range, the equilibrium lower limit which the roughing pump can achieve, the turbopump may be activated to further remove gas and vapor from the system. The system may then be baked and allowed to evacuate for several hours to ensure the vacuum pressure is optimally reduced as much as possible. The ion pump may then be activated to supplement or replace the turbo pump for holding vacuum during deposition or interferometer experiments.

A.2.3 Ion Cleaning

With the vacuum pressure reduced to $\sim 10^{-7}$ torr, the ion gun may be used for cleaning the sample. A controlled pressure of nitrogen or argon will be leaked into the chamber for the formation of ions during cleaning. Initially, the manual shutter will be covering the sample, and the linear shutter will be retracted away from the sample. The voltage potentials of the ion gun will be set to the appropriate levels and both electron and ion beam currents will be set to equivalent values and recorded. The sample stage will be steadily rotated by the motor to promote uniform cleaning of the sample. When the neutral ion beam current stabilizes to the desired level, the manual shutter may move away from the sample, exposing it to the incident ion beam. After a determined amount of time of exposure, the manual shutter will move back in front of the sample and the ion gun will be turned off gradually, reducing the voltage potential of the system to ground. The rotary sample motor may move the sample to the desired angular position, and the nitrogen or argon gas inlet will be closed, allowing the pressure to settle back down to high vacuum. The ion gun may also be incorporated into the deposition process through ion beam assisted deposition, which can affect the surface, density, and microstructure of the deposited thin films [40].

A.3 Deposition Procedure

A.3.1 *Preparing Evaporation System*

With the manual shutter covering the sample and linear shutter in desired position, the deposition process may be initiated. The steps for preparing the system are as follows.

1. Activate the deposition rate monitor by setting the appropriate voltage potential for the anode and cathode and preparing the ammeter for recording the ionization current, zeroing if necessary.
2. Set the potential difference between the crucible holding the deposition material, held at ground, and corresponding filament to establish the basis for thermionic emission.
3. Increase the filament current for the desired deposition metal gradually, observing the deposition rate monitor until reaching and stabilizing at the desired evaporation rate. Since the filament current supplies the electrons for thermionic emission, the transfer of kinetic energy of the electrons into thermal energy of the deposition metal will be gradual, thus the evaporation will take some time to begin and consequently settle into equilibrium.
4. Once the evaporation is maintained at the desired stable rate for several minutes, the actual deposition may begin.

A.3.2 *Aligning Shutters for Thickness Gradient*

Depending on the desired thickness gradient for the sample, the linear shutter may be initially extended in front of the sample and programmed to retract at a specified rate, or conversely initially retracted and programmed to extend in front of the sample; as the shutter gradually uncovers the sample to deposition, the surface exposed to the deposition for more time accumulates more deposited material, thus varying the thickness across the sample based on the deposition rate and time exposed. The linear shutter and sample motor may also be used in conjunction to create varying thin films on a single substrate. An example of this would be to cover half of the substrate with the linear shutter and deposit a film on the exposed side. Then, rotate the sample 180° to cover the newly deposited film and expose the remaining bare substrate for depositing a new film. The rotary motor may also be used to create films with radially uniform thickness; due to the nature of the evaporation of deposition material from the crucible, it is difficult to achieve uniform thickness across the entire surface of the substrate. For example, the flux of evaporated particles from the crucible will deposit at a rate proportional to $\cos \theta$, where θ is the angle from the perpendicular.

A.3.3 Performing Deposition

Once the deposition rate monitor indicates the desired value and the shutters are in the appropriate position, deposition is ready to commence. The manual rotary shutter will be moved to its vertical position, while the automated linear feedthrough shutter is concurrently activated to move to its preprogrammed positions at preprogrammed speeds. The user should carefully observe the deposition rate monitor for the duration of the deposition period, observing any changes in deposition rate to indicate the behavior of the deposition process. When the desired deposition has occurred, the manual rotary shutter may be swiftly moved to cover the substrate, thus ending deposition for this stage. The evaporation system may then be adjusted to the next appropriate settings, whether that be changing the deposition rate, changing deposition material, or simply ending deposition for the thin film. In general, the current and floating potential for the evaporation system should be adjusted gradually, and the deposition rate monitor will indicate the behavior of the evaporation system. For example, evaporation may continue to occur for a few seconds due to the accumulation of thermal energy even if the filament current is turned off; the deposition rate monitor should indicate there is no further deposition before switching to another deposition material or otherwise exposing the sample.

A.4 Post Deposition

When the complete deposition process is complete, the chamber may either be vented to remove the sample or kept under vacuum. The system may be kept under vacuum to perform interferometer experiments or simply store the sample for later.

A.5 Heating Experiments

A.5.1 Applications of Sample Heater

The substrate and sample temperature may be controlled and measured during any process using the sample heater apparatus. During deposition, the substrate may be increased in temperature to influence the thin film structure as it is deposited. After deposition, the sample may be annealed to supply the thermal energy required to stimulate grain growth. Further, the sample temperature may be controlled during interferometer experiments to measure the change in curvature as the sample temperature changes due to thermal stresses.

A.5.2 Sample Heater Procedure

When not performing deposition, the infrared heat mirror will be rotated to be positioned directly below the sample for heating experiments. The sample heater operates under the same method as the evaporation system, which uses thermionic emission from a filament to heat its respective crucible. In a similar manner, the heater will only operate under vacuum due to its tungsten filament. First, set the potential difference between the substrate and heater filament to a negative voltage using the floating supply. While observing the temperature of the substrate thermocouple, increase the heater filament current slowly until the temperature noticeably increases and settles to the desired level. It will take time for the temperature to increase and settle even while the filament current is constant, so the best method for controlling the substrate temperature will largely be careful trial and error.

A.5.3 Interferometer Experiments

The interferometer apparatus may be used in conjunction with the sample heater to directly measure the sample curvature at varying temperatures for thermal stress experiments. For interferometer experiments, the apparatus will need to be aligned to the initial substrate prior to deposition. After turning on the 25mW laser, the system may be adjusted using the three degrees of freedom supplied by the inner frame until the outgoing image from the substrate precisely overlaps the image from the reference mirror. Using a camera connected to a computer interface, an image of the substrate will be recorded prior to deposition to serve as a reference image, representing the initial state of the system. After deposition, the interferometer laser may be turned on and the images may be recorded every 5 seconds and processed by software to determine the phase shifts of each pixel and integrated to yield a topographical map of the sample as it changes. From each topographical map, the curvature of the film may be calculated both locally and non-locally for characterizing its stress through appropriate models.

REFERENCES

- [1] L. B. Freund, *J. Mech. Phys. Solids*, **48**, 1159 (2000).
- [2] X. Feng, Y. Huang, and A. Rosakis, *J. Appl. Mech.*, **74**, 1276 (2007).
- [3] L. B. Freund and S. Suresh, *Thin Film Materials*, (University Press, Cambridge, 2003). p. 86.
- [4] L. B. Freund and S. Suresh, *Thin Film Materials*, (University Press, Cambridge, 2003) p. 61.
- [5] L. B. Freund and S. Suresh, *Thin Film Materials*, (University Press, Cambridge, 2003). p. 83.
- [6] L. B. Freund and S. Suresh, *Thin Film Materials*, (University Press, Cambridge, 2003). p. 83.
- [7] D. L. Smith, *Thin Film Deposition* (McGraw-Hill, Inc., New York, 1995) p. 193.
- [8] L. N. Timian, Unpublished (2010).
- [9] G. G. Stoney, *Proc. R. Soc. Lond.*, **A82**, 172 (1909).
 ref: L. B. Freund and S. Suresh, *Thin Film Materials*, (University Press, Cambridge, 2003). p. 87.
- [10] D. Ngo, Y. Huang, A. J. Rosakis, and X. Feng, *Thin Solid Films*, **515**, 2220 (2006).
- [11] N. Guyot, Y. Harmand, and A. Mezin, *Int. J. Sci. Solids Struct.*, **41**, 5143 (2004).
- [12] M. Kobrinshy and C. Thompson, *Appl. Phys. Lett.*, **73** (17), 2429 (1998).
- [13] Y. Huang and A. Rosakis, *J. Mech. Phys. Solids*, **53**, 2483 (2005).
- [14] D. L. Smith, *Thin Film Deposition* (McGraw-Hill, Inc., New York, 1995). p. 188.
- [15] L. B. Freund and S. Suresh, *Thin Film Materials*, (University Press, Cambridge, 2003). p. 88.
- [16] D. L. Smith, *Thin Film Deposition* (McGraw-Hill, Inc., New York, 1995) pp. 188-192.
- [17] X. Feng, Y. Huang, and A. Rosakis, *J. Appl. Mech.*, **74**, 1276 (2007).
- [18] A. Brenner and S. Senderoff, *J. Res. Natl. Bur. Stand.*, **42**, 105 (1949).
 ref: L. B. Freund and S. Suresh, *Thin Film Materials*, (University Press, Cambridge, 2003). p. 98.
- [19] B. D. Harper and W. Chih-Ping, *J. Solids Struct.*, **26** (5-6), 511 (1990).
 ref: C. B. Masters and N. J. Salamon, *Int. J. Eng. Sci.*, **31** (6), 915 (1993).
- [20] T.-S. Park, S. Suresh, A. J. Rosakis, and J. Ryu, *J. Mech. Phys. Solids*, **51**, 2191 (2003).
- [21] C. B. Masters and N. J. Salamon, *Int. J. Eng. Sci.*, **31** (6), 915 (1993).
- [22] L. B. Freund, *J. Mech. Phys. Solids*, **48**, 1159 (2000).
- [23] L. B. Freund and S. Suresh, *Thin Film Materials*, (University Press, Cambridge, 2003). p. 181.
- [24] X. Feng, Y. Huang, and A. Rosakis, *J. Appl. Mech.*, **74**, 1276 (2007).
- [25] Y. Huang, D. Ngo, and A. Rosakis, *Acta Mech. Sin.*, **21**, 362 (2005).
- [26] D. Ngo, Y. Huang, A. Rosakis, and X. Feng, *Thin Solid Films*, **515**, 2220 (2006).
- [27] X. Feng, Y. Huang, and A. Rosakis, *J. Appl. Mech.*, **74**, 1276 (2007).
- [28] M. A. Brown et al, *Int. J. Solids Struct.*, **44**, 1755 (2007).

- [29] D. Ngo, Y. Huang, A. Rosakis, and X. Feng, *Thin Solid Films*, **515**, 2220 (2006).
- [30] X. Feng, Y. Huang, and A. Rosakis, *J. Appl. Mech.*, **74**, 1276 (2007).
- [31] N. Guyot, Y. Harmand, and A. Mezin, *Int. J. Sci. Solids Struct.*, **41**, 5143 (2004).
- [32] K. Chen and K. Ou, *J. Micromech. Microeng.*, **12** (6), 917 (2002).
- [33] T. Chen, W. Lin, and D. Chen, *J. Appl. Phys.*, **96** (7), 3800 (2004).
- [34] Y. Huang, D. Ngo, and A. Rosakis, *Acta Mech. Sin.*, **21**, 362 (2005).
- [35] T. Park et al., *J. Elec. Mat.*, **37**(6), 777 (2008).
- [36] L. B. Freund and S. Suresh, *Thin Film Materials*, (University Press, Cambridge, 2003) p. 184.
- [37] W. Breiland, S. R. Lee, and D. Koleske, *J. Appl. Phys.*, **95** (7), 3453 (2004).
- [38] T.-S. Park, S. Suresh, A. J. Rosakis, and J. Ryu, *J. Mech. Phys. Solids*, **51**, 2191 (2003).
- [39] H. A. Sodano and J-S. Bae, *J. Vib. Acous.*, **128**, 294 (2006).
- [40] K. Aikens, Unpublished (2009).